Architecture of petawatt-class z-pinch accelerators

W. A. Stygar,[1] M. E. Cuneo,[1] D. I. Headley,[2] H. C. Ives,[3] R. J. Leeper,[1] M. G. Mazarakis,[1] C. L. Olson,[1] J. L. Porter,[1]
T. C. Wagoner,[4] and J. R. Woodworth[1]

[1]*Sandia National Laboratories, Albuquerque, New Mexico 87185, USA*
[2]*American Staff Augmentation Providers, Albuquerque, New Mexico 87123, USA*
[3]*EG&G, Albuquerque, New Mexico 87107, USA*
[4]*Ktech Corporation, Albuquerque, New Mexico 87123, USA*
(Received 2 May 2006; published 21 March 2007)

We have developed an accelerator architecture that can serve as the basis of the design of petawatt-class z-pinch drivers. The architecture has been applied to the design of two z-pinch accelerators, each of which can be contained within a 104-m-diameter cylindrical tank. One accelerator is driven by slow ($\sim 1~\mu$s) Marx generators, which are a mature technology but which necessitate significant pulse compression to achieve the short pulses ($\ll 1~\mu$s) required to drive z pinches. The other is powered by linear transformer drivers (LTDs), which are less mature but produce much shorter pulses than conventional Marxes. Consequently, an LTD-driven accelerator promises to be (at a given pinch current and implosion time) more efficient and reliable. The Marx-driven accelerator produces a peak electrical power of 500 TW and includes the following components: (i) 300 Marx generators that comprise a total of 1.8×10^4 capacitors, store 98 MJ, and erect to 5 MV; (ii) 600 water-dielectric triplate intermediate-store transmission lines, which also serve as pulse-forming lines; (iii) 600 5-MV laser-triggered gas switches; (iv) three monolithic radial-transmission-line impedance transformers, with triplate geometries and exponential impedance profiles; (v) a 6-level 5.5-m-diameter 15-MV vacuum insulator stack; (vi) six magnetically insulated vacuum transmission lines (MITLs); and (vii) a triple-post-hole vacuum convolute that adds the output currents of the six MITLs, and delivers the combined current to a z-pinch load. The accelerator delivers an effective peak current of 52 MA to a 10-mm-length z pinch that implodes in 95 ns, and 57 MA to a pinch that implodes in 120 ns. The LTD-driven accelerator includes monolithic radial transformers and a MITL system similar to those described above, but does not include intermediate-store transmission lines, multimegavolt gas switches, or a laser trigger system. Instead, this accelerator is driven by 210 LTD modules that include a total of 1×10^6 capacitors and 5×10^5 200-kV electrically triggered gas switches. The LTD accelerator stores 182 MJ and produces a peak electrical power of 1000 TW. The accelerator delivers an effective peak current of 68 MA to a pinch that implodes in 95 ns, and 75 MA to a pinch that implodes in 120 ns. Conceptually straightforward upgrades to these designs would deliver even higher pinch currents and faster implosions.

PACS numbers: 84.70.+p, 84.60.Ve, 52.58.Lq

I. INTRODUCTION

A number of high-current z-pinch accelerators have been developed by the international pulsed-power community. These include SHIVA [1], Proto II [2–5], SuperMITE [5,6], Double EAGLE [7], Saturn [8,9], Angara 5 [10,11], Pegasus II [12–14], MAGPIE [15], Zebra [16,17], Atlas [18,19], Decade Quad [20,21], Z [22–31], and COBRA [32]. These machines have been used for a wide variety of inertial-confinement-fusion (ICF), radiation-physics, equation-of-state, plasma-physics, astrophysics, and other high-energy-density-physics experiments.

Presently, the z-pinch driver that operates at the highest electrical power is the Z accelerator, which is located at Sandia National Laboratories [22–31]. Z delivers 55 TW of electrical power to the accelerator's vacuum-insulator stack, and 19 MA to a 10-mm-initial-radius 10-mm-length pinch that implodes in 95 ns [33–43]. Such a pinch radiates 130 TW of x-ray power in a 12-ns pulse [33–43].

Recent calculations suggest that accelerators with electrical powers in excess of 1000 TW would be required to drive z-pinch implosions that radiate in excess of 1000 TW of x-ray power [42]. Such radiated powers would enable large-diameter ICF-capsule-implosion experiments [42–61] and other high-energy-density-physics experiments [62–68] to be conducted over heretofore inaccessible parameter regimes. Consequently, it is of interest to consider how a petawatt-class z-pinch accelerator might be designed.

A number of architectures have been proposed in the literature for the design of future pulsed-power z-pinch drivers [60,69–79]. In this article, we describe an architecture that was motivated by, and builds upon, the previous designs.

The architecture described herein can be driven by various types of electrical-pulse generators. We consider here two versions of the architecture: one driven by conventional Marx generators, and one driven by linear-transformer-driver (LTD) modules [60,74–76,79–102].

An LTD module is, in essence, a compact inductive voltage adder [103] in which each of the adder's cavities is driven by capacitors and switches contained within the cavity [60,74–76,79–102].

The Marx-based architecture includes the following: (i) several stacked levels of Marx generators; (ii) several stacked levels (one per Marx level) of water-dielectric triplate intermediate-store capacitors, which also serve as pulse-forming lines; (iii) two or more multimegavolt laser-triggered gas switches per Marx; (iv) several stacked levels (one per Marx level) of monolithic triplate radial-transmission-line impedance transformers, which are water insulated and have exponential impedance profiles; (v) a multilevel insulator stack; (vi) a multilevel system of magnetically insulated transmission lines (MITLs); and (vii) a post-hole vacuum convolute. (The gas switches used for the Marx generators, and the multimegavolt laser-triggered gas switches, would likely require the use of sulfur hexafluoride as the insulating gas.) This architecture assumes (i) no water switches; (ii) no long self-limited MITLs; (iii) no water convolute; and (iv) no plasma opening switches. The combination of these 11 features distinguish this architecture from the accelerator designs proposed in Refs. [60,69–79].

The radial impedance transformers offer a straightforward and efficient method of combining the outputs of several-hundred terawatt-level Marx-based pulse generators to produce a petawatt-level pulse. In addition, the transformers serve as passive high-pass filters which (along with the use of more than one laser-triggered gas switch per Marx) shorten the electrical-power pulse, and reduce the need for additional pulse-sharpening components, such as water switches or plasma-opening switches.

We note that the design of the *original* Proto-II accelerator [104], which was intended to drive electron-beam-diode loads, has several similarities to the Marx-based design described in this article. The original Proto II included a single 1.47-m-long triplate radial transformer with an exponential impedance profile [104]. However, this accelerator did not use triplate intermediate stores, or more than one gas switch per Marx. In addition, the intermediate stores were not used as pulse-forming lines, and water switches were used for pulse shaping [104].

Marx generators are a mature technology, but necessitate significant pulse compression to achieve the short pulses ($\ll 1~\mu$s) required to drive z pinches. LTDs are less mature, but produce much shorter pulses than conventional Marxes. Consequently, an LTD-driven accelerator promises to be, at a given pinch current and implosion time, more efficient and reliable. Seminal work by Kovalchuk *et al.* [80,83,88,92], Bastrikov *et al.* [81,90], Kim *et al.* [74,82,85,87,89,91,94,101], McDaniel and Spielman [84], Mazarakis *et al.* [76,79,86,102], Rose *et al.* [93,100], Vizir *et al.* [95], Leckbee *et al.* [96,97,99], and Rogowski *et al.* [98] have led to impressive advances in LTD technology.

As a result, LTDs are becoming an attractive alternative to conventional Marx generators.

The LTD-based architecture outlined in this article includes the following: (i) several stacked levels of LTD modules; (ii) a coaxial water-insulated matched-impedance transmission line within each LTD; (iii) several stacked levels (one per LTD level) of monolithic triplate radial-transmission-line impedance transformers, which are water insulated and have exponential impedance profiles; (iv) a multilevel insulator stack; (v) a multilevel MITL system; and (vi) a post-hole vacuum convolute. The design complexity of the LTD-based driver is significantly reduced relative to that of other accelerators, since it includes (i) no intermediate-store capacitors; (ii) no multimegavolt gas switches; (iii) no sulfur hexafluoride; (iv) no laser-trigger systems; (v) no pulse-forming transmission lines; (vi) no water switches; (vii) no long self-limited MITLs; (viii) no water convolute; and (ix) no plasma opening switches. The combination of the above 15 features distinguishes this architecture from the accelerator designs presented in Refs. [60,69–79].

The radial transformers offer a straightforward and efficient method of combining the outputs of several-hundred terawatt-level LTD-based pulse generators to produce a petawatt-level pulse. In addition, the transformers serve as passive high-pass filters, as they do for the Marx-based driver discussed above. Hence the transformers shorten the electrical-power pulse produced by the LTDs, and reduce the need for additional pulse-sharpening components.

LTDs have previously been proposed by Kim and Kovalchuk [74], McDaniel and Spielman [84], Corcoran and colleagues [75], Mazarakis and colleagues [76,79], and Olson [60] for use in future high-current z-pinch drivers. These proposals are the motivation for the consideration of LTDs in the present article.

The LTD-driven architecture described herein differs from the previous LTDs designs [60,74–76,79] in the following manner: (i) Each LTD module drives a concentric impedance-matched *water-dielectric* transmission line (as proposed by Corcoran and co-workers [75]), instead of a vacuum- or oil-insulated line; (ii) each such transmission line in turn drives a *monolithic triplate radial-transmission-line impedance transformer, which is water insulated and has an exponential impedance profile*; and (iii) each triplate impedance transformer connects directly, *without a water convolute*, to a triplate magnetically insulated transmission line located at the center of the accelerator.

The Marx-driven architecture is described in detail in Sec. II A. An elementary analytic model of an accelerator based on such an architecture is developed in Sec. II B. Scaling relations that estimate the peak pinch current as a function of other accelerator parameters are presented in Sec. II C.

The architecture described in Secs. II A, II B, and II C can be applied to the design of a wide variety of Marx-driven accelerators. In Sec. III A, for illustrative purposes, we apply this architecture to the conceptual design of a driver that produces a 500-TW electrical-power pulse, which is an order of magnitude greater than the electrical power presently achievable on Z [22–31,42]. Hence the 500-TW machine could serve as a useful and reasonable intermediate step between the Z accelerator and one capable of achieving high-yield fusion [42–61]. In Sec. III B, we discuss the reliability of a Marx-based machine.

The LTD-driven architecture is described in detail in Sec. IV A. An elementary analytic model of an accelerator based on such an architecture is developed in Sec. IV B. Scaling relations that estimate the peak pinch current as a function of other accelerator parameters are presented in Sec. IV C.

The architecture described in Secs. IV A, IV B, and IV C can be applied to the design of a wide variety of LTD-driven accelerators. In Sec. V A, we apply the architecture to the conceptual design of a driver that produces a 1000-TW electrical-power pulse. In Sec. V B, we discuss advantages of the LTD-driven accelerator over the Marx-based driver discussed in Sec. III A.

In Sec. VI we suggest how the accelerator designs outlined in Secs. II, III, IV, and V might be upgraded to achieve even higher electrical powers, and consequently higher pinch currents and faster implosions.

Sections II, III, IV, and V refer to auxiliary results presented in four Appendices. Appendix A discusses the performance of exponential impedance transformers. Appendix B estimates the optimum impedance of a transmission line connected to the output of a switch. Appendix C defines an *effective* value of the peak current delivered to a z pinch, and an *effective* pinch implosion time. In Appendix D, we estimate the optimum output impedance of the transmission line that is internal to, and is driven by, an idealized LTD module.

II. MARX-BASED ACCELERATOR ARCHITECTURE

A. Description

The Marx-based accelerator architecture is outlined in Fig. 1. Like that of many other z-pinch drivers, the architecture illustrated in the figure includes an oil section, a water section, and a vacuum section. The oil section encircles the water section, which in turn encircles the vacuum section. The three sections have cylindrical geometries, and are concentric.

As indicated by Fig. 1, the oil section includes several stacked levels of Marx generators. The outer diameter of the oil section, and the number of Marx levels, are determined by the requisite value of the initial energy storage, the maximum energy that can be stored per Marx capacitor, the dimensions of the Marx capacitors and switches, high-

voltage-insulation requirements, operational requirements, etc. The specific design outlined in Fig. 1 arbitrarily assumes 3 Marx levels.

The water section includes triplate intermediate-store transmission lines, multimegavolt laser-triggered gas switches, and monolithic triplate radial-transmission-line impedance transformers. The intermediate stores are pulse charged by the Marx generators as the Marx's erect. When the voltage across the intermediate stores is near its peak value, the gas switches are triggered, which launches an electrical-power pulse at the input to the monolithic transformers. A radially converging power pulse subsequently propagates in the transformers toward the vacuum section, which is located at the center of the accelerator. (The *triplate* radial transformers proposed here are similar to the *biplate* transformer proposed by Petr and co-workers for generating a high-voltage pulse applicable to particle acceleration [105].)

In this article, we assume that each radial transformer has an exponential impedance profile [106,107]; i.e., that in each transformer,

$$\frac{1}{Z_t} \frac{dZ_t}{dr} = \text{const}, \qquad (1)$$

where Z_t is the radially dependent impedance of the transformer and r is the radial coordinate. In such a transformer the *fractional* change in the impedance per unit length is constant. Exponential transformers are more efficient than those with a linear impedance profile; i.e., those for which $(dZ_t/dr) = \text{const}$ [106,107]. However, it appears that the impedance profile that *optimizes* the performance of a transmission-line transformer is not known [106,107]. Lewis and Wells [106] suggest that the performance of a Gaussian transformer may be superior to that of an exponential transformer; however, the latter is easier to treat theoretically. For the discussions in this article, we do not explore improvements to the exponential design.

The vacuum section of Fig. 1 consists of a 6-level vacuum-insulator stack, 6 magnetically insulated transmission lines (MITLs), a triple-post-hole vacuum convolute, and a z-pinch load. The insulator stack serves as the water-vacuum interface. The stack and MITLs of Fig. 1 have 6 levels to match the 6 radial transmission lines (i.e., the 3 radial triplates) in the water section, and the 3 Marx levels in the oil section. The currents at the outputs of the 6 MITLs are added by the vacuum convolute; the combined current is delivered by the convolute to the z-pinch load. The convolute outlined in Fig. 1 is a three-level version of the double-post-hole convolute described in Refs. [108–117].

The large-diameter monolithic radial-transmission-line impedance transformers outlined in Fig. 1 are one of the most distinguishing features of the accelerator architecture described in this article. The transformers offer the follow-
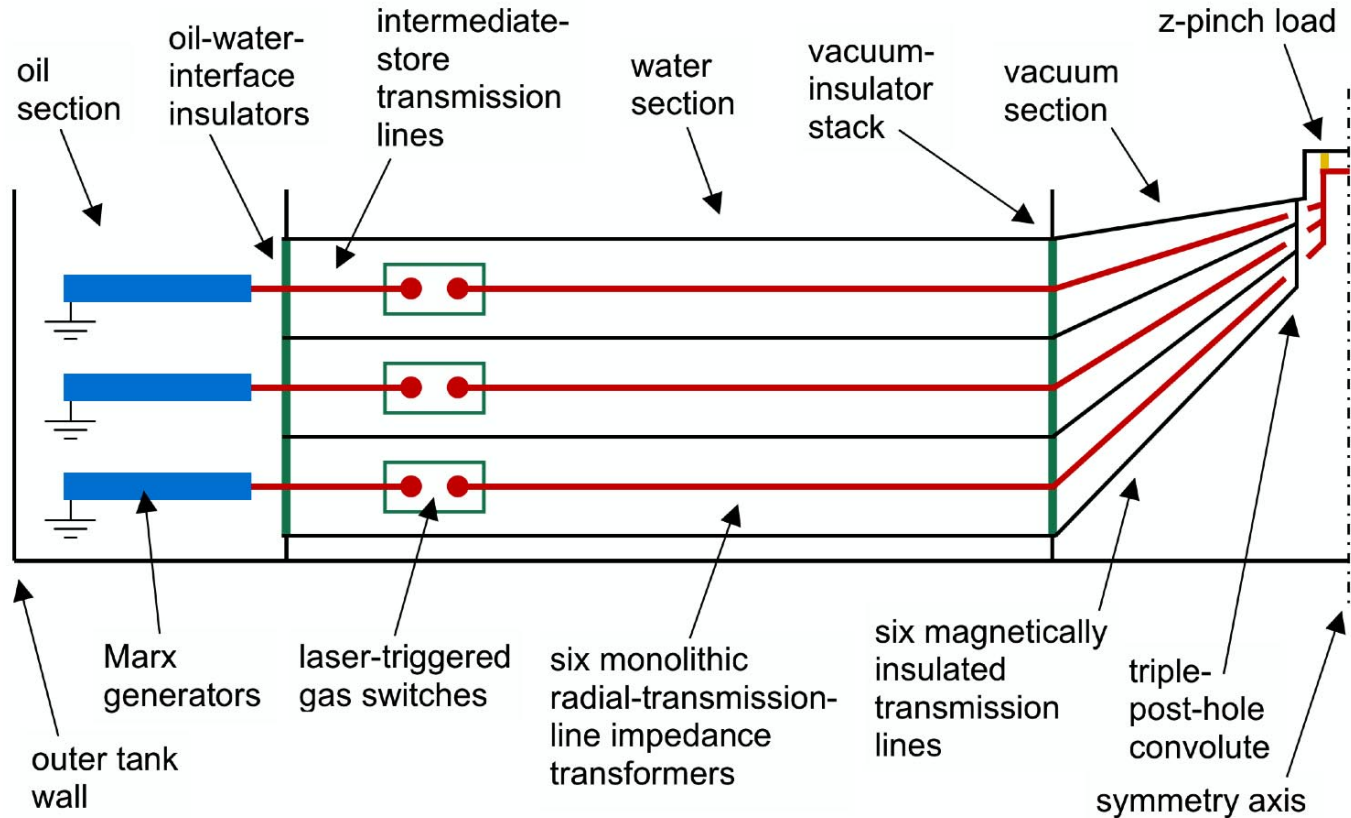
FIG. 1. (Color) Conceptual design of a Marx-based petawatt-class *z*-pinch driver. The anode electrodes are black; the cathodes are red. This particular design includes 3 levels of Marx generators, 6 intermediate-store transmission lines (3 triplates), 6 monolithic radial-transmission-line impedance transformers (3 triplates), a 6-level vacuum-insulator stack, 6 magnetically insulated transmission lines, a triple-post-hole vacuum convolute, and a *z*-pinch load. The anode-cathode gaps of the water-insulated transformers are shown here as being independent of radius; however, the actual gaps would likely vary to achieve an exponential impedance profile. (The drawing is not to scale.)

ing advantages over previous approaches to the design of a high-current *z*-pinch accelerator [60,69–79].

(i) The radial transformers of Fig. 1 offer a straightforward, efficient, and relatively inexpensive method of combining the outputs of several-hundred terawatt-level electrical-pulse generators to produce a petawatt-level pulse [105]. The pulse generators can be Marx-based generators, as assumed in Secs. II and III, or the LTD-based generators assumed in Secs. IV and V.

(ii) For Marx-based accelerators, the flat triplate geometry of the intermediate stores and radial transformers enable the use of more than one laser-triggered gas switch per Marx. Increasing the number of switches in this manner reduces the total inductance and resistance of the gas-switch system, which narrows the width of the forward-going power pulse. Consequently, there is less need for the inefficient self-break water switches used in other accelerator designs for pulse sharpening. Not only are water switches inefficient, they also launch a pressure pulse in the water, which can damage nearby hardware.

(iii) The impedance at the input of the radial transformers can be chosen to maximize the electrical power that is transferred from the pulse generators to the radial transformers.

(iv) The impedance at the output of the radial transformers can be chosen to maximize the power transferred from the radial lines to the accelerator's stack-MITL system.

(v) Since the radial lines are transformers, they increase the voltage generated by the electrical-pulse generators to the voltage required to drive the stack-MITL system [105]. Consequently, the transformers eliminate the need for voltage-adding hardware, such as crossover networks and transit-time-isolated transmission-line adders, which are assumed by other accelerator designs. The requisite voltage transformation is performed directly by the radial transformers, since the number of transformers is chosen to be identical to the number of MITLs.

(vi) Since the radial lines are transformers, and since their one-way transit time is much longer than the temporal width of power pulses of interest, the transformers also serve as passive high-pass filters [105,106]. In a Marx-based accelerator, the radial transformers reduce the pre-pulse created by the slow (∼ 1 μs) charging of the inter-

mediate stores by the Marxes. The transformers also sharpen the forward-going power pulse, in addition to the sharpening described in paragraph (ii) above. Such pre-pulse reduction and sharpening further reduce the need for self-break water switches. The performance as a function of frequency of an *idealized* exponential transformer is discussed in Appendix A.

(vii) The radial lines smooth azimuthal variations in the forward-going power pulses generated by the electrical-pulse generators. Such variations are caused by statistical differences in the times at which the pulses are launched, and differences in the powers produced by the pulse generators. The smoothing reduces the probability that such fluctuations can significantly weaken magnetic insulation in the vacuum-section transmission lines.

(viii) The radial lines make it possible to *shape* the load current, for applications that require a specific load-current waveform. Shaping can be achieved by phasing the times at which the electrical-pulse generators launch their forward-going pulses. The pulses would be smoothed azimuthally by the time they arrive at the vacuum-section transmission lines.

(ix) The anodes of the radial lines shown in Fig. 1 can be *effectively* monolithic and relatively flat. Hence, such transmission lines do not require significant geometric enhancements of the electric field at the anodes, where dielectric breakdown in water is most likely to initiate [118]. Of course, each of the transmission-line anodes and cathodes would not be monolithic in the strictness sense; i.e., each electrode would not be fabricated from a single sheet of metal. We expect that, due to fabrication issues, the radial lines would be divided into several sections. We also expect that there would be several wide radial slots cut in the cathode electrodes to achieve the desired exponential impedance profiles, and also for diver access. There would, in addition, be holes in the anodes for diver access; however, these could be closed during an accelerator shot.

(x) The relatively flat geometry of the anodes and cathodes makes them relatively inexpensive to fabricate.

(xi) The relatively closed geometry of the radial lines reduces considerably electromagnetic-radiation losses, which improves accelerator efficiency.

(xii) The relatively closed geometry shields experimental, diagnostic, and facility hardware from the electromagnetic pulse produced by the accelerator.

B. Analytic model of a Marx-based accelerator

For a given application, the optimum parameters of the accelerator components outlined in Fig. 1 might be best determined through iterative numerical simulations. To begin such simulations, it is useful to have *initial analytic estimates* of the requisite parameters. Estimates that are accurate to *at most, first order*, are presented below.

For the discussion below, we assume that the application requires that the accelerator drive a z-pinch load. We assume that the desired peak pinch current, pinch implosion time, pinch length, and initial pinch radius are given by I, τ_i, ℓ, and R, respectively. These parameters determine the requisite value of the pinch mass m, which is approximately given by the following expression [40,42]:

$$m = (1.81 \times 10^{-8}) \frac{I^2 \tau_i^2 \ell}{R^2} \text{ kg.} \qquad (2)$$

(Equations are in SI units throughout.)

The desired values of I and τ_i determine the requisite values of the peak electrical power at the stack P_s and the peak stack voltage V_s. Under the conditions studied in Ref. [42], these variables are related as follows:

$$P_s = (4.23 \times 10^{-18}) \frac{I^{8/3}}{\tau_i^{5/3}} \text{ W,} \qquad (3)$$

$$V_s = (4.54 \times 10^{-18}) \left(\frac{I}{\tau_i} \right)^{5/3} \text{ V.} \qquad (4)$$

Equations (3) and (4) assume that the minimum value of the initial stack-MITL inductance L_s required for reliable accelerator operation is approximately given by the following empirical relation [42]:

$$L_s = (3.29 \times 10^{-11}) V_s^{2/5} \text{ H.} \qquad (5)$$

We caution that the constants on the right-hand sides of Eqs. (2)–(5) are valid only when the *shapes* of the pinch-current, stack-power, and stack-voltage waveforms are *mathematically similar* to the shapes assumed for the analysis presented in Ref. [42]. We also caution that the constant on the right-hand side of Eq. (3) is a sensitive function of the phase difference between the voltage and current at the stack; hence *in general* Eq. (3) can only be accurate *to zeroth order*. In addition, we note that Eq. (5) implicitly assumes the use of anode plugs [119,120] in the insulator stack. (Two electrodes bound each of the insulators in an insulator stack. An anode plug is an extension of the anode electrode into the insulator; the resulting shaped electrode serves as a partial Faraday cage that reduces the field at the anode triple junction [119,120].) Equation (5) also assumes that the stack-flashover probability is limited to $\sim 10^{-3}$, as calculated by the statistical insulator-flashover model developed in Ref. [121].

The electrical power P_s is delivered to the stack-MITL system by the water-section radial transformers illustrated by Fig. 1. To first order, the output impedance of the transformer system $Z_{t,o}$ that maximizes the transfer of electrical energy from the transformers to the stack and MITLs is [71]

$$Z_{t,o} \sim 1.1 \frac{L_s}{\tau_i}. \qquad (6)$$

For the idealized conditions assumed by Ref. [71], the optimum impedance $Z_{t,o} \sim 2L_s/\tau_i$. This expression is obtained by assuming L_s is held constant as $Z_{t,o}$ is varied. However, L_s is an increasing function of the stack voltage V_s, as suggested by Eq. (5). For the conditions considered herein, we find from numerical circuit simulations that Eq. (6) provides a somewhat more accurate estimate for the optimum value of $Z_{t,o}$.

The accelerator illustrated in Fig. 1 assumes 6 water-section radial-transmission-line transformers that are electrically in parallel. For an accelerator with n_t such transformers, the impedance of the transformer system at its output (i.e., at the outer radius of the vacuum-insulator stack) is given by the following:

$$Z_{t,o} = \frac{60}{n_t \varepsilon^{1/2}} \left(\frac{g_{t,o}}{r_{t,o}} \right) \Omega. \tag{7}$$

In the above expression ε is the dielectric constant of water, $g_{t,o}$ is the anode-cathode (AK) gap at the output of each of the n_t transformers, and $r_{t,o}$ is the radius at the output of the transformers.

The electric field in the transformers is highest near their output; i.e., near the insulator stack. To minimize the probability of water-dielectric breakdown, we require that the peak value (in time) of the mean electric field at the output $E_{t,o}$ satisfies the following relation [122]:

$$E_{t,o} \tau_{t,o}^{0.330} \leq 1.13 \times 10^5, \tag{8}$$

where

$$E_{t,o} \equiv \frac{V_s}{g_{t,o}}, \tag{9}$$

and $\tau_{t,o}$ is the full width of the voltage pulse (at the output) at 63% of peak [122]. {The appearance of Eq. (8) differs from that of Eq. (11) in Ref. [122] since we use SI units in the present article.} The overall energy efficiency of the accelerator is, of course, optimized when

$$\tau_{t,o} \sim \tau_i. \tag{10}$$

Equation (9) uses the peak voltage *at* the stack. The peak voltage in the radial transformers is actually higher just *outside* the stack due to that part of the power pulse that is reflected from the stack. However, for systems of interest, the transformer AK gaps will likely be larger in this region (to achieve the exponential impedance profile). In addition, the effective pulse width of the voltage is shorter here than at the stack. Numerical calculations suggest that (for systems of interest) if the criterion given by Eq. (8) is met *at* the stack it will also be met *near* the stack. Hence in this article we simply assume Eq. (8), and caution that a more complete analysis should verify that Eq. (8) is also satisfied in the radial transformers near the stack.

When Eq. (6) is satisfied; i.e., when $Z_{t,o}$ is well matched to the stack-MITL inductance for implosion times of in-terest, then

$$P_s \sim P_{f,o}, \tag{11}$$

where

$$P_{f,o} = \frac{V_{f,o}^2}{Z_{t,o}} \tag{12}$$

is the peak forward-going power at the output of the transformers, and $V_{f,o}$ is the peak forward-going voltage.

For the conditions assumed in Appendix A, transmission-line transformers are reasonably efficient and *approximately* conserve electrical power. Under such conditions we can write

$$P_{f,o} = \frac{V_{f,o}^2}{Z_{t,o}} = \eta \frac{V_{f,i}^2}{Z_{t,i}} = \eta P_{f,i}, \tag{13}$$

where η is the power efficiency of the transformers, $V_{f,i}$ is the peak forward-going voltage at the input of the transformers, $Z_{t,i}$ is the impedance of the transformer system at its input, and $P_{f,i}$ is the peak forward-going input power.

As suggested by Fig. 1, the electrical-power pulse at the input of the transformers is delivered by the intermediate-store transmission lines. As shown in Appendix B, the input impedance of the transformer system $Z_{t,i}$ that maximizes the forward-going power launched at the system's input is given by

$$Z_{t,i} = Z_{IS,o} + R_{eff}, \tag{14}$$

where $Z_{IS,o}$ is the output impedance of the system of intermediate stores and

$$R_{eff} \sim \frac{L_g}{\tau_g} + R_g. \tag{15}$$

In this expression L_g is the inductance of the system of laser-triggered gas switches, τ_g is the width of the pulse incident upon the switches (which is approximately equal to the two-way transit time of an intermediate-store transmission line), and R_g is the characteristic resistance of the system of switches. The overall energy efficiency of the accelerator is optimized when

$$\tau_g \sim \tau_i. \tag{16}$$

Assuming that there are n_t radial transformers, the impedances $Z_{t,i}$ and $Z_{IS,o}$ are given as follows:

$$Z_{t,i} = \frac{60}{n_t \varepsilon^{1/2}} \left(\frac{g_{t,i}}{r_{t,i}} \right), \tag{17}$$

$$Z_{IS,o} = \frac{60}{n_t \varepsilon^{1/2}} \left(\frac{g_{IS}}{r_{IS,o}} \right), \tag{18}$$

where $g_{t,i}$ is the AK gap at the input of each of the n_t transformers, $r_{t,i}$ is the radius at the input to the transformers, g_{IS} is the AK gap of each of the intermediate

stores, and $r_{IS,o}$ is the radius at the intermediate-store output. (We assume that the AK gap of an intermediate store is constant throughout its length.)

For the Marx-based accelerator considered in Sec. III A, we can (to first order) ignore the length of a gas switch; hence, we make the simplifying assumption that

$$r_{t,i} = r_{IS,o}. \tag{19}$$

Since τ_g is approximately equal to the two-way transit time of an intermediate-store transmission line, we also have that

$$r_{IS,i} = r_{IS,o} + \frac{c\tau_g}{2\varepsilon^{1/2}}, \tag{20}$$

where c is the speed of light.

The intermediate stores are typically charged on a time scale that is long compared to the time required to close the gas switches. Hence we assume that the peak intermediate-store voltage V_{IS} is the same throughout the length of each of the stores, which implies that at peak voltage, the peak *forward-going* voltage in the stores is $V_{IS}/2$. Using this assumption, Eq. (14), and Eq. (B8), we find that the peak forward-going voltage at the input to the radial impedance transformers $V_{f,i}$ is approximately

$$V_{f,i} \sim \frac{V_{IS}}{2}. \tag{21}$$

The actual value of $V_{f,i}$ is somewhat greater than that predicted by Eq. (21) since the intermediate stores are still charging when the gas switches fire.

To minimize the probability of dielectric breakdown in the intermediate stores, we require that the peak value (in time) of the mean electric field in the stores E_{IS} satisfies the following relation [122]:

$$E_{IS}\tau_{IS}^{0.330} \leq 1.13 \times 10^5, \tag{22}$$

where

$$E_{IS} \equiv \frac{V_{IS}}{g_{IS}}. \tag{23}$$

The quantity τ_{IS} is the full width of the voltage pulse, at 63% of peak, across the IS anode-cathode gaps [122]. The pulse width is determined in part by the circuit parameters of the Marx generators, which pulse charge the intermediate stores.

It is straightforward to show that the transfer of energy from the Marxes to the intermediate stores is maximized when

$$\frac{\tau_g}{Z_{IS,i} + Z_{IS,o}} = C_{IS} \lesssim C_M, \tag{24}$$

where $Z_{IS,i}$ is the input impedance of the system of intermediate stores, C_{IS} is the capacitance of the IS system, and C_M is the capacitance of the system of Marx generators (after they have erected). The capacitance C_M is given by

$$C_M = \frac{n_M C_{cap}}{n_{cap}}, \tag{25}$$

where n_M is the number of Marx generators, C_{cap} is the capacitance of a single Marx capacitor, and n_{cap} is the number of capacitors in each Marx. The value of C_M given by Eq. (24) is somewhat larger than C_{IS} because of the resistance of the Marx generators. In the absence of resistive losses, and assuming that there is an inductor between the Marx generators and intermediate stores, all the Marx energy is transferred to the intermediate stores when $C_{IS} = C_M$.

When Eqs. (24) and (25) are satisfied,

$$V_{IS} \sim V_M \equiv n_{cap} V_{cap}, \tag{26}$$

where V_M is the nominal peak voltage achieved by the erected Marx generators, and V_{cap} is the initial DC voltage to which each of the Marx capacitors is charged. The total initial energy stored in the Marx generators E_M can be expressed as

$$E_M = \tfrac{1}{2}C_M V_M^2 = \tfrac{1}{2}n_M n_{cap} C_{cap} V_{cap}^2. \tag{27}$$

Additional information needs to be provided to close the above system of equations. For the accelerator design outlined in Sec. III A, we make the following simplifying assumptions:

$$\varepsilon = 80, \tag{28}$$

$$n_t = 6, \tag{29}$$

$$\eta = 0.8, \tag{30}$$

$$L_g = \frac{400 \text{ nH}}{n_g}, \tag{31}$$

$$R_g = \frac{200 \text{ m}\Omega}{n_g}, \tag{32}$$

$$n_g = 2n_M, \tag{33}$$

$$V_{IS} = 5 \text{ MV}, \tag{34}$$

$$\tau_{IS} = 410 \text{ ns}, \tag{35}$$

$$n_{cap} = 60, \tag{36}$$

$$C_{cap} = 1.34 \ \mu\text{F}, \tag{37}$$

$$V_{cap} = 90 \text{ kV}. \tag{38}$$

As indicated by Eqs. (7), (17), and (18), the requisite value of the AK gap of a transmission line increases as $\varepsilon^{1/2}$. Hence, water is an attractive insulating medium because its high dielectric constant (~ 80) reduces consid-

erably the electric field in the transformers and intermediate stores [118]. For this reason, we assume Eq. (28).

The accelerator design described in Sec. III A assumes 6 radial-line transformers [Eq. (29)]. The Z accelerator uses, in effect, 4 transmission-line levels [22–31], hence an increase to 6 appears to be a reasonably conservative step. A detailed study would be required to determine the optimum value of n_t for a given set of conditions.

As discussed in Appendix A, the *intrinsic* power efficiency of the transformer system for the Marx-based driver discussed in Sec. III A is 83%. This assumes that the water resistivity $\rho_w = 3\,\text{M}\Omega$-cm, and that losses due to the transformer-electrode resistance and the imaginary component of the water permittivity can be neglected. Equation (30) makes the simplifying assumption that for accelerators of interest, $\eta = 0.8$.

Equations (31) and (32) assume that the characteristic inductance and resistance of each laser-triggered gas switch are 400 nH [123] and 200 mΩ [124], respectively. The quantity n_g [Eq. (33)] is the total number of gas switches that can be installed in the accelerator, which is determined by $r_{t,i}$ (the radius at which the switches are located) and various engineering constraints. For the Marx-based accelerator considered in this article, it appears we can assume Eq. (33).

Equation (34) assumes that the gas switches can be operated reliably when the peak intermediate-store voltage is 5 MV, which is approximately the operating voltage of the switches presently in use on the Z accelerator [123]. (According to Ref. [123], the Z gas switches can be operated reliably at 5.0–5.2 MV.) Equation (35) is obtained from numerical circuit simulations for the design described in Sec. III A; these assume that the series resistance and inductance of a single Marx are 3.74 Ω and 15.5 μH, respectively [124]. Equation (36) assumes that each Marx generator consists of 60 capacitors; Eq. (37) that each Marx capacitor has a capacitance of 1.34 μF; and Eq. (38) that each Marx capacitor is initially charged to 90 kV. Equations (34)–(38) are essentially identical to the Marx parameters of the Z accelerator [123–125].

Although not directly relevant to the *electrical* design of an accelerator, it is useful to obtain an estimate of the outer radius of the accelerator's oil tank. For the Marx-based accelerator considered in Sec. III A, we find that the requisite minimum value of the outer tank radius r_{tank} can be approximated as

$$r_{\text{tank}} = r_{\text{IS},i} + 6.5\text{ m.} \qquad (39)$$

C. Scaling of I with other accelerator parameters

The above equations can be used to determine how the peak pinch current I scales with other accelerator parameters. Combining Eqs. (3) and (11)–(13), we find that

$$I \propto (\eta P_{f,i})^{3/8} \tau_i^{5/8}. \qquad (40)$$

Combining Eqs. (13)–(16), (21), (24), (26), (27), and (40), and assuming

$$\frac{L_g}{\tau_g} \ll Z_{\text{IS},o}, \qquad (41)$$

$$R_g \ll Z_{\text{IS},o}, \qquad (42)$$

Cuneo obtains [126]

$$I \propto (\eta E_{\text{M}})^{3/8} \tau_i^{1/4}. \qquad (43)$$

According to Eqs. (40) and (43), the peak current I does not scale simply as $P_{f,i}^{1/2}$ and $E_{\text{M}}^{1/2}$, since Eq. (3) assumes that the requisite minimum value of the initial stack-MITL-system inductance L_s scales as indicated by Eq. (5) [42].

Assuming Eqs. (13)–(15), (18), (21), and (40)–(42), that $Z_{\text{IS},i} \sim Z_{\text{IS},o}$, and also that

$$V_{\text{IS}} \propto g_{\text{IS}} \qquad (44)$$

in order to satisfy Eq. (22), we obtain the following:

$$I \propto (\eta n_t r_{\text{IS},o} V_{\text{IS}})^{3/8} \tau_i^{5/8}. \qquad (45)$$

[Equation (45) assumes ε is held constant.] Equations (20), (39), and (45) suggest that, for given values of I, η, n_t, and τ_i, the outer tank radius r_{tank} could be decreased if the intermediate-store voltage V_{IS} is increased.

III. MARX-BASED ACCELERATOR DESIGN

A. 100-ns 500-TW driver

We have applied the architecture outlined in Sec. II and Fig. 1 to the conceptual design of a z-pinch accelerator that produces a 100-ns 500-TW electrical-power pulse. The accelerator parameters for this design are summarized in Table I, which describes three options. The design of the accelerator itself is held constant for these options; the only difference between these is the design of the z-pinch load.

Iterative numerical circuit simulations were performed to develop an optimized circuit model of the accelerator. *Initial* estimates of the accelerator-circuit parameters (which were used to initiate the simulations) were determined assuming Eqs. (1)–(38); the desired z-pinch parameters were arbitrarily assumed to be as follows:

$$I \sim 50\text{ MA,} \qquad (46)$$

$$\tau_i = 95\text{ ns,} \qquad (47)$$

$$\ell = 10\text{ mm,} \qquad (48)$$

$$R = 10\text{ mm.} \qquad (49)$$

ARCHITECTURE OF PETAWATT-CLASS *z*-PINCH ...

Phys. Rev. ST Accel. Beams **10,** 030401 (2007)

TABLE I.   Accelerator and *z*-pinch parameters for three Marx-based-accelerator options. The parameters are compared to those of the existing *Z* accelerator [22–31,40,42]. For these options the design of the accelerator itself is identical; the options differ only due to differences in the *z*-pinch loads. For the *Z* accelerator and all three higher-current options, the initial pinch radius is assumed to be 10 mm. The nominal values of the peak pinch implosion velocity and kinetic energy assume a 10:1 pinch-radius convergence ratio. The effective peak pinch current and effective implosion time are defined in Appendix C.

Accelerator and pinch parameters	Present *Z* accelerator	Marx-accelerator option 1	Marx-accelerator option 2	Marx-accelerator option 3
Outer tank diameter $2r_{\text{tank}}$	33 m	104 m	104 m	104 m
Number of pulse generators	36 5.4-MV Marx generators	300 5.4-MV Marx generators	300 5.4-MV Marx generators	300 5.4-MV Marx generators
Initial energy storage	12 MJ	98 MJ	98 MJ	98 MJ
Peak intermediate-store voltage V_{IS}	5 MV	5 MV	5 MV	5 MV
$E_{\text{IS}}\tau_{\text{IS}}^{0.330}$	0.94×10^5	1.09×10^5	1.09×10^5	1.09×10^5
Number of laser-triggered gas switches n_g	36	600	600	600
Nominal charge transferred per laser-triggered gas switch	120 mC	60 mC	60 mC	60 mC
Number of impedance transformers n_t	4	6	6	6
Water resistivity ρ_w	1.5 MΩ/cm	3.0 MΩ/cm	3.0 MΩ/cm	3.0 MΩ/cm
Insulator-stack radius $r_{t,o}$	1.8 m	2.7 m	2.7 m	2.7 m
Initial inductance of the stack-MITLsystem L_s	13 nH	24 nH	24 nH	24 nH
Peak electrical power at the stack P_s	55 TW	520 TW	520 TW	520 TW
Peak stack voltage V_s	3.1 MV	15 MV	15 MV	15 MV
$E_{t,o}\tau_{t,o}^{0.330}$	1.18×10^5	1.1×10^5	1.1×10^5	1.1×10^5
Effective peak pinch current I_{eff}	19 MA	52 MA	57 MA	43 MA
Actual peak pinch current I	19 MA	48 MA	53 MA	42 MA
Energy delivered to the stack at *z*-pinch stagnation	3.3 MJ	38 MJ	42 MJ	35 MJ
Length of the *z*-pinch load ℓ	10 mm	10 mm	10 mm	20 mm
Z-pinch mass m	5.9 mg	43 mg	83 mg	59 mg
Effective pinch implosion time $\tau_{i,\text{eff}}$	95 ns	95 ns	120 ns	95 ns
Nominal peak pinch implosion velocity v_p	47 cm/μs	47 cm/μs	37 cm/μs	47 cm/μs
Nominal peak pinch kinetic energy E_k	0.65 MJ	4.8 MJ	5.8 MJ	6.6 MJ
Estimated total radiated x-ray energy	1.6 MJ	12 MJ	14 MJ	16 MJ

Equations (46)–(49) correspond to the pinch parameters of option 1 (Table I). The simulations were conducted using the SCREAMER circuit code [127]. The *z*-pinch load was modeled in SCREAMER as an imploding cylindrical foil with a perfectly stable and infinitely thin wall.

The parameters given by Eqs. (46)–(49) are of interest for *z*-pinch-driven ICF experiments [42–61]. The peak current and implosion time given by Eqs. (46) and (47), respectively, would enable ICF-capsule-implosion and *z*-pinch-physics experiments of fundamental importance to the design of a high-thermonuclear-yield facility.

We developed the circuit to satisfy approximately the constraints given by Eqs. (1), (5)–(10), (14)–(29), (31)–(34), (36)–(38), and (46)–(49). Under these conditions we determined numerically optimum values of $r_{\text{IS},i}$, $r_{\text{IS},o}$, $r_{t,i}$, $r_{t,o}$, $Z_{\text{IS},i}$, $Z_{\text{IS},o}$, $Z_{t,i}$, and $Z_{t,o}$. We define the optimum values to be those which maximize the efficiency of delivering energy from the Marx generators to the *z*-pinch load, consistent with the constraints given by Eqs. (46)–(49). The numerical simulations find that the optimum values are *approximately* as follows:

$$r_{\text{IS},i} = 45.4 \text{ m}, \qquad (50)$$

$$r_{\text{IS},o} = r_{t,i} = 43.9 \text{ m}, \qquad (51)$$

$$r_{t,o} = 2.7 \text{ m}, \qquad (52)$$

$$Z_{\text{IS},i} = 8.9 \text{ m}\Omega, \qquad (53)$$

$$Z_{\text{IS},o} = 9.2 \text{ m}\Omega, \qquad (54)$$

$$Z_{t,i} = 16.2 \text{ m}\Omega, \qquad (55)$$

$$Z_{t,o} = 260 \text{ m}\Omega. \qquad (56)$$

For the conditions described above, the requisite number of Marx generators n_{M} is 300. Since there are two intermediate-store transmission lines per Marx, the impedance of each intermediate store is 5.4 Ω.

The *analytic* accelerator model of Sec. II B assumes that the efficiency of the radial transformer is $\eta = 0.8$ [Eq. (30)]. The *numerical* simulations do not make this assumption, and instead include a 1D model of the transformer in the circuit model, and calculate the transformer efficiency. The simulations include effects due to the exponential impedance profile and resistivity of the water, but neglect losses due to electrode resistance and the imagi-

nary component of the water permittivity. The impedance transformer defined by Eqs. (51), (52), (55), and (56) is discussed further in Appendix A.

As suggested by Table I, the simulations assume that the water resistivity ρ_w is 3.0 MΩ-cm. This is a factor of 2 higher than the nominal resistivity routinely achieved on the *Z* accelerator. Presently, the water used in *Z* is processed by resin beds; Cuneo [128] has proposed the use of a reverse-osmosis electrodeionization treatment for the petawatt-class accelerators considered here. Such a treatment may achieve resistivities on the order of 3.0 MΩ-cm, even though the water volume of a petawatt accelerator would be an order of magnitude greater than it is for *Z*.

The numerical simulations do not assume Eq. (32), but instead that the gas-switch resistance falls from a high initial value to 200 mΩ in an exponential decay with a 10-ns time constant [124,127]. Similarly the numerical simulations do not assume Eq. (35), but instead that the series resistance and inductance of a single Marx are 3.74 Ω and 15.5 μH, respectively [124]. In addition, the simulations assume that electron-flow effects in the MITLs can be modeled as discussed in Ref. [29], and that the flow impedance of the MITL system is 0.5 Ω.

The results of the numerical simulations described above are summarized in Table I in the column titled "Marx-accelerator option 1." This column lists *effective* values of the peak pinch current and implosion time, which are defined in Appendix C.

The optimized accelerator circuit described above was used to drive two other *z*-pinch loads, in addition to the load defined by Eqs. (46)–(49). In this manner we obtained the accelerator-pinch parameters listed in the columns labeled as options 2 and 3 in Table I. The pinch *geometry* for option 2 is identical to that of option 1; however, the pinch *mass* of option 2 was chosen to be that which gives a 120-ns effective implosion time. The pinch of option 3 has twice the length of option 1; the mass of option 3 was chosen to achieve the same implosion time as for option 1.

The numerical simulations predict that for these three options, the *peak* values (in time) of the pinch current, stack voltage, stack energy, and stack power would be as listed in Table I. Also listed in the table are the predicted pinch implosion velocities and kinetic energies. The *time-dependent* stack current, pinch current, stack voltage, and stack energy for option 1 are plotted in Fig. 2.

Experiments conducted on the *Z* accelerator [40,42] demonstrate that the total x-ray energy radiated by a pinch with the parameters listed in the *Z*-accelerator column of Table I is 1.6 MJ, which is a factor of 2.46 greater than the *nominal* pinch kinetic energy of 0.65 MJ that is obtained by a circuit simulation. Assuming *optimistically* that the radiated x-ray energy is proportional to $I_{\text{eff}}^2 \ell$ [40,42], we obtain the x-ray yields listed in the table for options 1–3. {Because I_{eff} is defined by Eq. (C6), the x-ray yields given
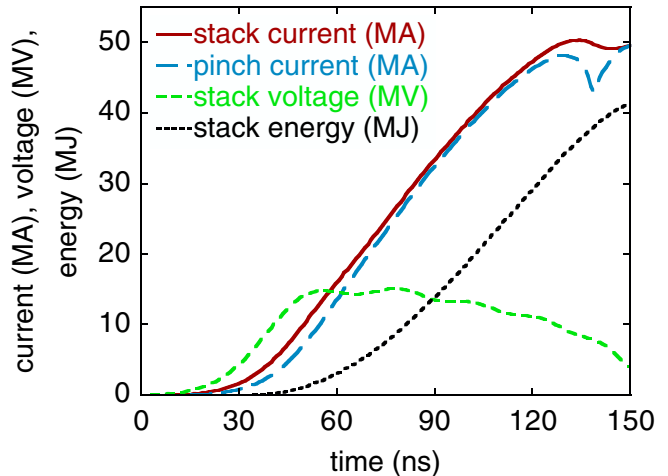

FIG. 2. (Color) The stack current, pinch current, stack voltage, and stack energy for the Marx-based accelerator referred to as option 1 in Table I.

in the table implicitly assume that the yield is *proportional* to the *nominal* pinch kinetic energy [40,42]. However, we caution that under the conditions studied in Refs. [40,42], the measured total radiated x-ray energy is proportional to $I^{1.73 \pm 0.18}$.}

B. Accelerator reliability

The requisite Marx-generator and laser-triggered-gas-switch performance parameters listed in Table I for the 500-TW accelerator are comparable to the parameters presently achieved on *Z* [123–125]. However, the reliability of the *Z* components may have to be improved before they can be applied to the 500-TW driver.

For example, the present *Z* laser-triggered gas switch has a ~1% failure rate. Since 600 switches would be used on the 500-TW accelerator, on average 6 switches would fail every shot. (The actual failure rate might be lower than this, since as indicated by Table I, the 500-TW machine would transfer a factor of 2 less charge per switch per shot than is transferred by the present *Z* accelerator.)

It might be possible to design the 500-TW accelerator so that, if a few gas switches fail per shot, the compromised switches could be electrically isolated from the accelerator circuit before the subsequent shot. The accelerator could then be fired until its forward-going power is reduced ~5%, at which time a day or two could be reserved to drain the water section for repairs. Assuming a 1% switch failure rate and that a 5% power reduction is acceptable, the water would have to be drained every 5 shot days.

Each of the laser-triggered gas switches assumed for the 500-TW machine would require an ultraviolet-laser-trigger system. The present lifetime of such a system on the *Z* accelerator is on the order of 100 shots; similar considerations apply to this system as well.

IV. LTD-BASED ACCELERATOR ARCHITECTURE

A. Description

The LTD-based accelerator architecture is outlined in Figs. 3 and 4. The architecture illustrated in these figures includes an LTD section, a water section, and a vacuum section. The LTD section encircles the water section, which in turn encircles the vacuum section. The three sections have cylindrical geometries, and are concentric.

As indicated by Figs. 3 and 4, the LTD section includes several stacked levels of LTD-driven electrical-pulse generators. Each LTD pulser, which we refer to as an "LTD module" to be consistent with the standard nomenclature, is a linear array of stacked annular LTD "stages" in a voltage-adding configuration. An LTD stage is also referred to as a "cavity."

The LTD-module design we consider in this article consists of a stack of 60 cavities [74,79]. Figure 5 illustrates how a 3-cavity module would function. The circuit model illustrated by Fig. 5 is that proposed by Mazarakis and colleagues in Refs. [76,79,86].

The outer diameter of the accelerator's LTD section is determined by the length of each LTD module, the number of modules, and the number of LTD levels. The length of each module is determined by the length of each LTD cavity and the number of cavities per module. The total number of cavities is determined by the power produced by each cavity, and the total electrical power required of the accelerator. Figures 3 and 4 arbitrarily assume 3 LTD levels.

The water section of Figs. 3 and 4 consists of 3 stacked monolithic radial-transmission-line impedance transformers, with triplate geometries. We assume the transformers have exponential impedance profiles (which we do not attempt to illustrate in the figures). The LTD modules launch an electrical-power pulse at the input to the transformers. A radially converging power pulse subsequently propagates in the transformers toward the vacuum section, which is located at the center of the accelerator. We assume the use of radial transformers for the LTD-based architecture for the reasons listed in paragraphs (i) and (iii)–(xii) of Sec. II A.

The vacuum section of Figs. 3 and 4 consists of a 6-level vacuum-insulator stack, 6 MITLs, a triple-post-hole vacuum convolute, and a *z*-pinch load. The insulator stack serves as the water-vacuum interface. The stack and
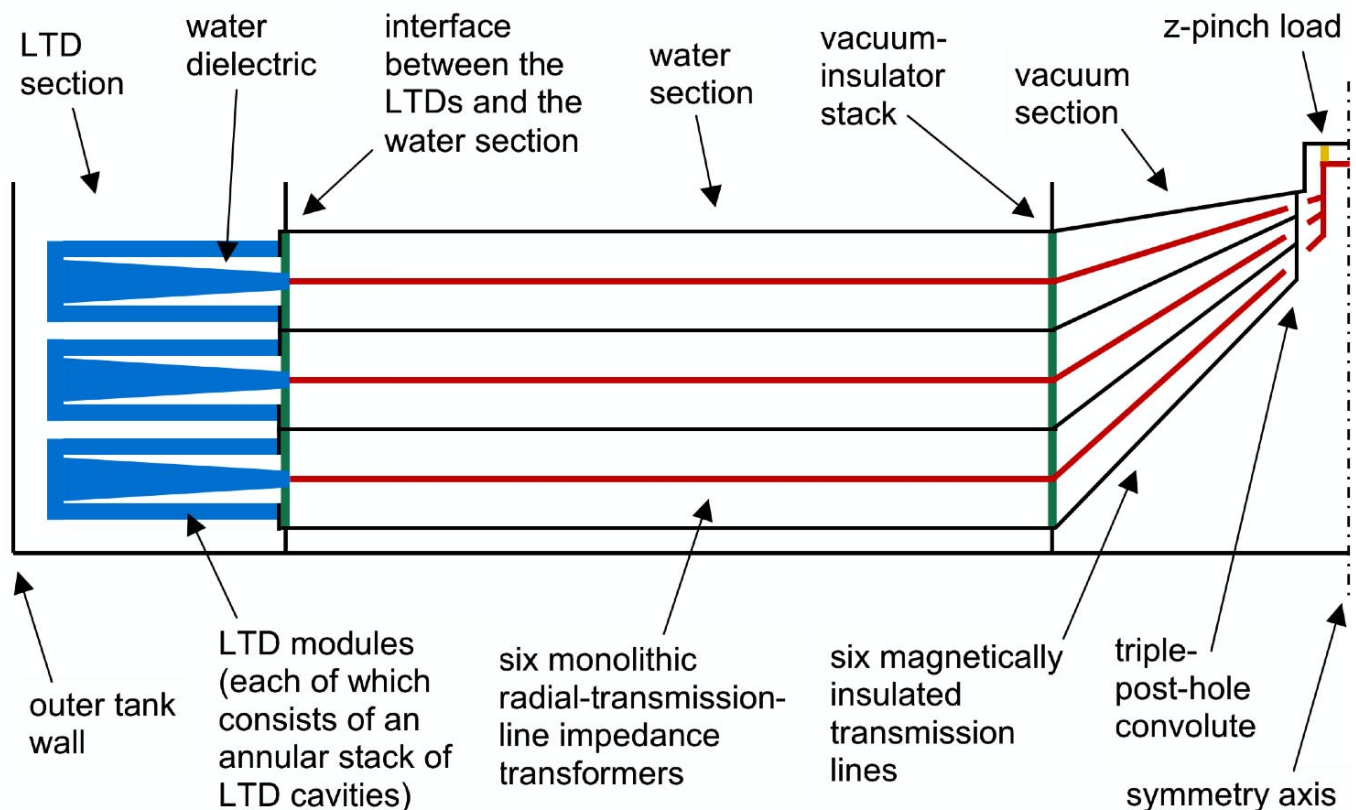

FIG. 3. (Color) Conceptual design of an LTD-based petawatt-class *z*-pinch driver. The design illustrated here is identical to that outlined in Fig. 1, except that the Marx generators, intermediate stores, and gas switches of Fig. 1 have been replaced by linear transformer drivers (LTDs) [60,74–76,79–102]. The anode-cathode gaps of the water-insulated transformers are shown here as being independent of radius; however, the actual gaps would likely vary with radius to achieve an exponential impedance profile. (The drawing is not to scale.)
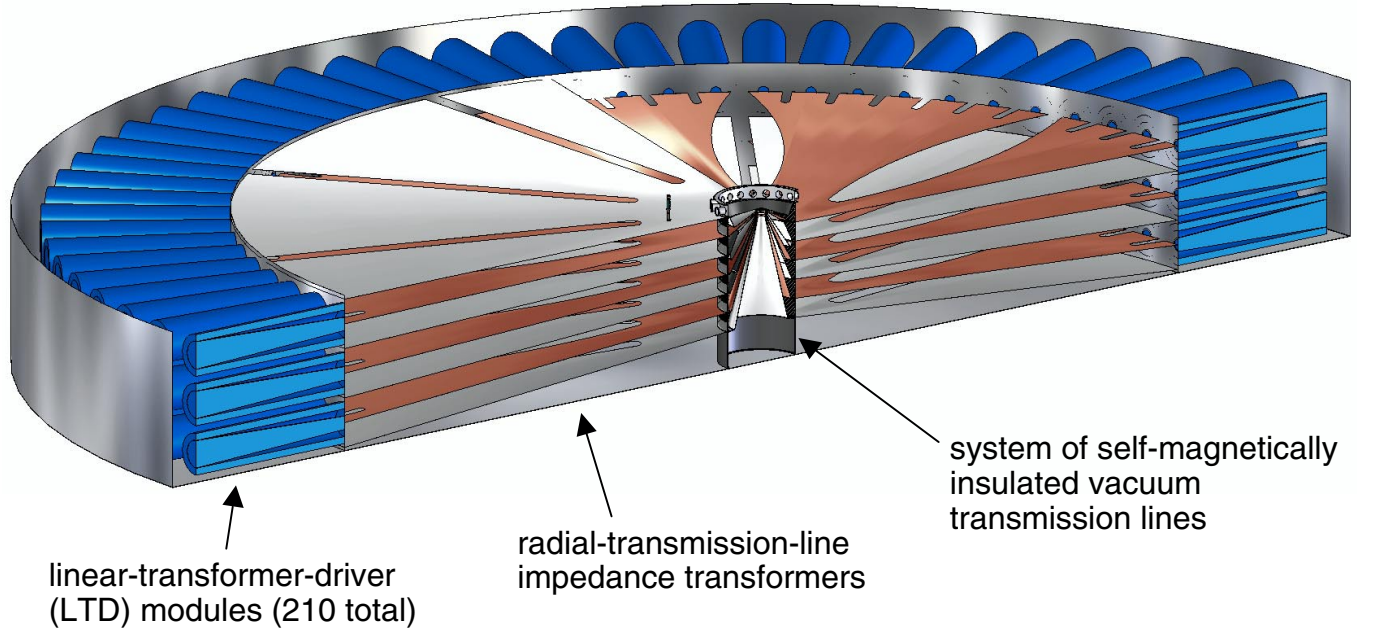
FIG. 4. (Color) Three-dimensional model of a 1000-TW LTD-based *z*-pinch accelerator. The model is approximately to scale. The diameter of the outer-tank wall is 104 m [79]. The model shows a person standing on the uppermost water-section electrode, near the central vacuum section.

MITLs of Figs. 3 and 4 have 6 levels to match the 6 radial transmission lines (i.e., the 3 radial triplates) in the water section, and the 3 LTD levels in the LTD section. The currents at the outputs of the 6 MITLs are added by the vacuum convolute; the combined current is delivered by the convolute to the *z*-pinch load. The convolute is assumed to be a 3-level version of the double-post-hole convolute described in Refs. [108–117].

B. Analytic model of an LTD-based accelerator

Like the analytic model described in Sec. II B, the LTD-accelerator model described in the present section is accurate to, at most, first order. The model includes Eqs. (1)–(13), (17), and (28)–(30), which are also applicable to an LTD-based driver. We complete these equations as follows.

Mazarakis and colleagues [76,79,86] have observed that an LTD module and its associated internal coaxial transmission line can, under the conditions illustrated by Fig. 5, be *approximately* modeled as a single series *RLC* circuit that drives a constant-impedance transmission line. This model, which is correct to first order, neglects losses due to the imperfect nature of the LTD's magnetic cores, which are not addressed herein. Considerably more complete circuit models of an LTD cavity are presented by Kim and colleagues in Ref. [94] and Leckbee and co-workers in Ref. [99].

Assuming the idealized *RLC*-circuit model [76,79,86], we find in Appendix D that the peak value in time of the forward-going power at the output of an LTD's internal transmission line is optimized when the output impedance of the line Z_{mod} is given by the following expression:

$$Z_{\mathrm{mod,opt}} = n_{\mathrm{cav}}\left(1.10\sqrt{\frac{L_{\mathrm{cav}}}{C_{\mathrm{cav}}}} + 0.80R_{\mathrm{cav}}\right). \qquad (57)$$

The quantity n_{cav} is the number of LTD cavities in the module; the quantities L_{cav}, C_{cav}, and R_{cav} are the series inductance, capacitance, and resistance of a single cavity, respectively. In the sense defined above [94], an LTD module is impedance matched to its internal transmission line when $Z_{\mathrm{mod}} = Z_{\mathrm{mod,opt}}$. Equation (57) is consistent to within 14% with the circuit-simulation results presented in Fig. 5 of Ref. [94]. The 14% discrepancy is due primarily to the neglect of magnetic-core losses by Eq. (57).

We find numerically that, when Eq. (57) is satisfied and $\sqrt{L_{\mathrm{cav}}/C_{\mathrm{cav}}} \gg R_{\mathrm{cav}}$, the forward-going power launched by a system of LTD modules is approximately

$$P_{f,i} \sim \frac{0.33n_{\mathrm{LTD}}n_{\mathrm{cav}}^2V_{\mathrm{cav}}^2}{Z_{\mathrm{mod,opt}}}, \qquad (58)$$

where n_{LTD} is the number of LTD modules and V_{cav} is the initial charge voltage of a single LTD cavity. We also find that the temporal width of the forward-going LTD power pulse is approximately

$$\tau_{\mathrm{LTD}} \sim 1.6\sqrt{L_{\mathrm{cav}}C_{\mathrm{cav}}}. \qquad (59)$$

The efficiency of an LTD-driven pinch-accelerator system is of course optimized when

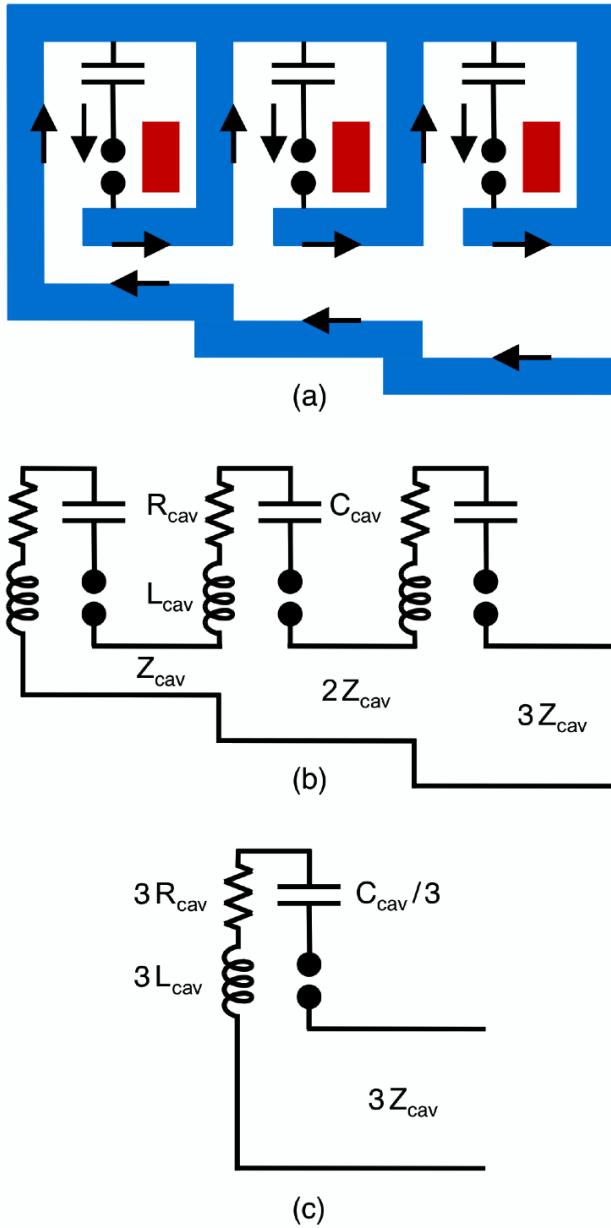$$\tau_{\mathrm{LTD}} \sim \tau_i. \qquad (60)$$

(a)

(b)

(c)

FIG. 5. (Color) (a) Idealized representation of a 3-cavity LTD module. Each cavity contains 80 capacitors and 40 switches; these are represented here by a single capacitor and a single switch. The red rectangles represent magnetic cores. The arrows represent the path of *most* of the current flow, after all the switches in the cavities have closed. We neglect here the small fraction of the current that flows around the inductive cores. The LTD module assumed in Secs. IV and V consists of 60 cavities. (b) Circuit diagram of the 3-cavity module, neglecting losses due to the cores [76,79,86]. (c) Equivalent circuit model of the module [76,79,86]. This circuit is valid only when the switches of a given cavity close at a time that is τ_{cav} later than the closure of the switches in the cavity immediately to the left, where τ_{cav} is the time it takes an electromagnetic pulse to propagate (down the transmission line) the length of a single cavity. Hence τ_{cav} is the one-way transit time of a single transmission-line segment. We assume here that all the cavities, and all the transmission-line segments, have the same electrical length.

The transfer of electrical power from a system of n_{LTD} LTD modules to a system of impedance transformers with input impedance $Z_{t,i}$ is optimized when

$$Z_{t,i} = \frac{Z_{\text{mod,opt}}}{n_{\text{LTD}}}. \qquad (61)$$

The total initial energy stored in the system of LTD modules is given by

$$E_{\text{LTD}} = \tfrac{1}{2} n_{\text{LTD}} n_{\text{cav}} C_{\text{cav}} V_{\text{cav}}^2. \qquad (62)$$

Consequently,

$$E_{\text{LTD}} \propto P_{f,i} \tau_i. \qquad (63)$$

To close the above system of equations for an LTD-based accelerator, we make the following assumptions:

$$r_{t,i} = \frac{d_{\text{cav}} n_{\text{LTD}}}{\pi n_t}, \qquad (64)$$

$$d_{\text{cav}} = 3.3 \text{ m}, \qquad (65)$$

$$n_{\text{cav}} = 60, \qquad (66)$$

$$C_{\text{cav}} = 800 \text{ nF}, \qquad (67)$$

$$L_{\text{cav}} = 7.5 \text{ nH}, \qquad (68)$$

$$R_{\text{cav}} = 15 \text{ m}\Omega, \qquad (69)$$

$$V_{\text{cav}} = 190 \text{ kV}. \qquad (70)$$

The quantity d_{cav} is the diameter of the space required by an LTD cavity. Presently the LTD cavities of most interest for driving z pinches are those described by Kim and colleagues [94] and Mazarakis and co-workers [79]; these cavities have a diameter of 3 m. Equation (64) allows an extra 0.3 m of space between cavities. We note that, according to Eqs. (13) and (21)–(23), the maximum values of $V_{f,i}$ and $P_{f,i}$ are, for a Marx-based accelerator, limited in part by water breakdown. For many LTD-driven accelerators of interest, $P_{f,i}$ [Eq. (58)] is instead limited in part by d_{cav}, which in turn determines the maximum possible packing fraction and hence n_{LTD} [Eq. (64)].

Equation (29) makes the arbitrary assumption that there are 3 LTD levels (which implies $n_t = 6$); Eq. (66) assumes each LTD module consists of 60 cavities. A more detailed study would be required to determine the optimum values of n_t and n_{cav} for a given set of conditions.

Presently the cavities of most interest [79,94] each have a series capacitance C_{cav} of 800 nF, as assumed by Eq. (67).

(Each such cavity contains 80 40-nF capacitors altogether, which are arranged as 40 capacitor *pairs* in parallel. Each pair consists of two capacitors in series. Each pair of capacitors is connected to a single switch, so that each cavity includes 40 switches.) According to Refs. [79,94], each such cavity has an inductance of 5.8 nH; we make the arbitrary and conservative assumption that, when such cavities are produced in large quantities, cost and fabrication issues might increase the inductance to 7.5 nH [Eq. (68)]. The larger inductance has the benefit of lengthening the rise time of the LTD output pulse, which reduces the peak voltage at the stack. (Alternatively, the rise time could be increased by increasing C_{cav}.) The internal resistance of each cavity is given in Refs. [79,94] as 15 mΩ [Eq. (69)]. The LTD cavities can be charged to 200 kV using a $+100$ kV, -100 kV charging system [79,94]; since we do not model magnetic-core losses [94,99] in the cavities, Eq. (70) assumes $V_{cav} = 190$ kV.

The length of each of the LTD cavities assumed herein is 22.15 cm [79,94]. Hence the length of a 60-cavity LTD module would be 13.29 m.

C. Scaling of *I* with other accelerator parameters

Equation (40) gives the scaling of I with respect to η, $P_{f,i}$, and τ_i for a Marx-driven accelerator; this equation is also applicable to an LTD-based driver. According to Eqs. (40) and (63), the scaling of I with respect to E_{LTD} and τ_i is given by

$$I \propto (\eta E_{LTD})^{3/8} \tau_i^{1/4}, \qquad (71)$$

which is analogous to Eq. (43).

When Eqs. (40), (57)–(60), and (64) are applicable and $\sqrt{L_{cav}/C_{cav}} \gg R_{cav}$, then

$$I \propto \left(\frac{\eta n_t n_{cav} r_{t,i}}{d_{cav}} \right)^{3/8} C_{cav}^{1/2} L_{cav}^{1/8} V_{cav}^{3/4}. \qquad (72)$$

Equation (72) suggests I can be increased by increasing both C_{cav} and L_{cav}; however, increasing these quantities also increases the width of the LTD power pulse since $\tau_{LTD} \propto \sqrt{L_{cav} C_{cav}}$ [Eq. (59)].

V. LTD-BASED ACCELERATOR DESIGN

A. 100-ns 1000-TW driver

The architecture outlined in Sec. IV, Fig. 3, and Fig. 4 has been applied to the conceptual design of an LTD-based *z*-pinch accelerator that delivers a 100-ns 1000-TW pulse to the accelerator's insulator stack. The parameters of the design are summarized in Table II.

Iterative numerical circuit simulations were performed to develop an optimized circuit model of the accelerator. *Initial* estimates of the accelerator-circuit parameters (which were used to initiate the simulations) were determined assuming Eqs. (1)–(13), (17), (28)–(30), and (57)–(70). The desired *z*-pinch parameters were arbitrarily

chosen to be as follows:

$$I \sim 65 \text{ MA}, \qquad (73)$$

$$\tau_i = 95 \text{ ns,} \qquad (74)$$

$$\ell = 10 \text{ mm,} \qquad (75)$$

$$R = 10 \text{ mm.} \qquad (76)$$

Equations (73)–(76) correspond to the pinch parameters of option 1 of Table II. The simulations were conducted using the SCREAMER circuit code [127].

We developed the circuit to satisfy approximately the constraints given by Eqs. (1), (5)–(10), (17), (28), (29), (57)–(62), (64)–(70), and (73)–(76). Under these conditions, and assuming that the maximum stack radius $r_{t,o}$ presently achievable in a reasonable manner is 3 m, we determined numerically optimum values of $r_{t,i}$, $Z_{t,i}$, and $Z_{r,o}$. We define the optimum values to be those which maximize the efficiency of delivering energy from the LTD modules to the *z*-pinch load, under the constraints given by Eqs. (73)–(76). These values are approximately as follows:

$$r_{t,i} = 36.9 \text{ m,} \qquad (77)$$

$$Z_{t,i} = 33.9 \text{ m}\Omega, \qquad (78)$$

$$Z_{t,o} = 360 \text{ m}\Omega. \qquad (79)$$

For the conditions described above, the requisite number of LTD modules n_{LTD} is 210.

The numerical simulations described in this section differ from the analytic model of Sec. IV B in the same manner that the simulations of Sec. III A differ from the analytic model of Sec. II B. The impedance transformer defined by Eqs. (77)–(79) and the constraint $r_{t,o} = 3$ m is discussed in more detail in Appendix A.

The results of the numerical simulations are summarized in the column titled "LTD-accelerator option 1" of Table II. This column lists *effective* values of the peak pinch current and implosion time, which are defined in Appendix C.

The optimized accelerator circuit described above was used to drive two other *z*-pinch loads, in addition to the load described by Eqs. (73)–(76). In this manner we obtained the accelerator-pinch parameters listed in the columns of Table II labeled as options 2 and 3. The pinch *geometry* for option 2 is identical to that of option 1; the pinch *mass* of option 2 was chosen to be that which gives an effective implosion time of 120 ns. The pinch of option

TABLE II.   Accelerator and *z*-pinch parameters for three LTD-based-accelerator options. The parameters are compared to those of the existing *Z* accelerator [22–31,40,42]. For these options the design of the accelerator itself is identical; the options differ only due to differences in the *z*-pinch loads. For the *Z* accelerator and all three higher-current options, the initial pinch radius is assumed to be 10 mm. The nominal values of the peak pinch implosion velocity and kinetic energy assume a 10:1 pinch-radius convergence ratio. The effective peak pinch current and effective implosion time are defined in Appendix C.

Accelerator and pinch parameters	Present *Z* accelerator	LTD-accelerator option 1	LTD-accelerator option 2	LTD-accelerator option 3
Outer tank diameter $2r_{\text{tank}}$	33 m	104 m	104 m	104 m
Number of pulse generators	36 5.4-MV Marx generators	210 11.4-MV LTDs	210 11.4-MV LTDs	210 11.4-MV LTDs
Initial energy storage	12 MJ	182 MJ	182 MJ	182 MJ
Number of impedance transformers n_t	4	6	6	6
Water resistivity ρ_w	1.5 MΩ/cm	3.0 MΩ/cm	3.0 MΩ/cm	3.0 MΩ/cm
Insulator-stack radius $r_{t,o}$	1.8 m	3.0 m	3.0 m	3.0 m
Initial inductance of the stack-MITL system L_s	13 nH	29 nH	29 nH	29 nH
Peak electrical power at the stack P_s	55 TW	1050 TW	1050 TW	1050 TW
Peak stack voltage V_s	3.1 MV	24 MV	24 MV	24 MV
$E_{t,o}\tau_{t,o}^{0.330}$	1.18×10^5	1.1×10^5	1.1×10^5	1.1×10^5
Effective peak pinch current I_{eff}	19 MA	68 MA	75 MA	59 MA
Actual peak pinch current I	19 MA	63 MA	70 MA	57 MA
Energy delivered to the stack at *z*-pinch stagnation	3.3 MJ	77 MJ	88 MJ	73 MJ
Length of the *z*-pinch load ℓ	10 mm	10 mm	10 mm	20 mm
Z-pinch mass m	5.9 mg	74 mg	146 mg	111 mg
Effective pinch implosion time $\tau_{i,\text{eff}}$	95 ns	95 ns	120 ns	95 ns
Nominal peak pinch implosion velocity v_p	47 cm/μs	47 cm/μs	37 cm/μs	47 cm/μs
Nominal peak pinch kinetic energy E_k	0.65 MJ	8.3 MJ	10 MJ	12 MJ
Estimated total radiated x-ray energy	1.6 MJ	20 MJ	25 MJ	30 MJ

3 has twice the length of option 1; the mass was chosen to achieve the same implosion time as for option 1.

The numerical simulations predict that for these three options, the *peak* values in time of the pinch current, stack power, stack voltage, and stack energy would be as listed in Table II. Also listed in Table II are predicted pinch implosion velocities, kinetic energies, and total radiated x-ray yields. (The x-ray yields listed for options 1–3 of Table II are calculated as described in the last paragraph of Sec. III A.) The *time-dependent* stack current, pinch current, stack voltage, and stack energy for option 1 are plotted in Fig. 6.

The total forward-going electrical power launched by the 210 LTD modules (which consist of 12 600 LTD cavities) at the input of the radial impedance transformers is 1230 TW, or approximately 0.1 TW per cavity. This is the peak power predicted by our idealized LTD circuit model, which makes the conservative assumption that $V_{\text{cav}} = 190$ kV to cover the small magnetic-core losses that the model neglects. The 1230-TW prediction is consistent with the considerably more complete calculations—and the measurements—described by Kim and colleagues in Ref. [94]. The results presented in Ref. [94] suggest that each of the LTD cavities assumed by the present article can in fact produce a peak electrical power of ~0.1 TW.

Of the 1230 TW launched at the input to the transformers, approximately 1000 TW arrives at the vacuum insulator stack, as indicated by Table II.

B. Advantages of the LTD-based accelerator

In this section we discuss advantages of the LTD-based accelerator outlined in Sec. V A over the Marx-based driver described in Sec. III A.

We assume conventional slow (~ 1 μs) Marx generators in Sec. III A since such Marxes are a mature technology. However, slow Marxes require additional pulse-compression circuitry to achieve the fast (≪ 1 μs) pulses required to drive *z*-pinch implosions [42]. Section III A assumes this circuitry consists of intermediate-store capacitors (which also serve as pulse-forming lines) and multimegavolt laser-triggered gas switches.

The 600 laser-triggered gas switches of Fig. 1 would operate at 5 MV. Hence, assuming the scenario outlined in Sec. III B, it would be necessary to drain the entire water section of Fig. 1 every 5 shot days for repairs. Each of the 600 switches would be triggered by an ultraviolet-laser-trigger system; these would also require that the water section be drained for repairs. Even if the gas switches and laser-trigger systems assumed for the Marx-based
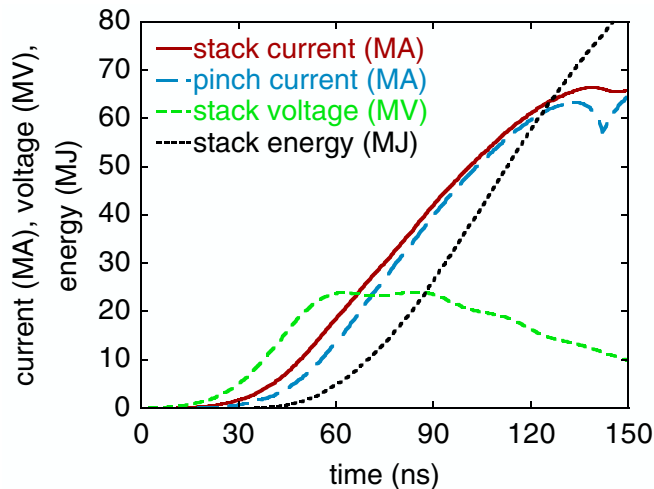
FIG. 6. (Color) The stack current, pinch current, stack voltage, and stack energy for the LTD-based accelerator referred to as option 1 in Table II.

driver could be made extremely reliable, this accelerator would require that 600 laser alignments be performed or verified before every accelerator shot.

We consider now the LTD-based accelerator outlined in Sec. V A. As suggested by Figs. 3 and 4, the water section of the LTD driver would be completely passive, since it would not contain any switches. Hence, it would be necessary to drain the water section only when an insulating rod (as might be used to separate the water-section electrodes) becomes damaged. Such infrequent draining would facilitate maintaining the water resistivity at a high level, which would increase the efficiency of the water-section impedance transformers.

The LTD machine described in Sec. V A would require 504 000 electrically triggered gas switches in a series-parallel configuration. (Each of the 12 600 LTD cavities would contain 40 switches connected in parallel.) However, each LTD switch would transfer only 7% of the charge that would be transferred by each of the laser-triggered gas switches assumed in Sec. III A; in addition, each LTD switch would operate at only 4% of the voltage. Hence each LTD switch would transfer only 0.2% of the energy. Consequently, although the LTD accelerator would require a much larger number of switches than the Marx driver, it is reasonable to expect that the LTD switches could be made significantly more reliable than the multi-megavolt switches of the Marx accelerator.

In fact, the consideration of LTDs as drivers for a petawatt-class accelerator is motivated in part by the following observation: The *effective* reliability of a *system* of switches is inversely proportional to the average fractional reduction (due to switch failure) per shot in the peak accelerator power. Hence the *effective system reliability* might be *improved* by using a large number of extremely reliable low-voltage switches, rather than a smaller number of higher-voltage switches.

The LTD-cavity design assumed for this article is described by Kim and colleagues in Ref. [94] and Mazarakis and co-workers in Ref. [79]. This cavity uses the advanced gas switches developed by Kovalchuk, Kim, Bastrikov, and colleagues [74,80–83,85,87–92,94,101]. When operated at 170–190 kV, these switches have a lifetime in excess of 3×10^4 shots [129] and a random failure rate less than 7×10^{-6} [129,130]. Assuming the failure rate is 7×10^{-6}, 3.5 LTD switches would fail per shot, compared to 6 for the Marx driver. The *fractional* reduction in the forward-going power per shot may be as low as $\sim 7 \times 10^{-6}$ for the LTD driver, *3 orders of magnitude less* than the 10^{-2} reduction for the Marx-based machine. Hence even though the LTD driver has far more switches, the effective reliability would be greater for the LTD accelerator than for the Marx-based machine.

In addition, the LTD switches assumed herein run on dry air, and do not require sulfur hexafluoride [74,80–83,85,87–92,94,101]. Moreover, the LTD switches are electrically triggered and do not require an ultraviolet-laser-trigger system; hence the maintenance, repair, and alignment of such a system is eliminated.

We also note that the LTD cavities assumed in Sec. IV B, Sec. V A, and Appendix D [76,94] are more energy efficient than conventional Marx-based pulse generators, and that the cavities can be fired every ~ 10 s [130]. These characteristics are of great interest for inertial-fusion-energy applications [60]. Furthermore, as noted by Kim [131], an LTD-driven accelerator would be more flexible than a Marx-based driver, since the former includes a large number of cavities that can, if desired, be rearranged to produce a different accelerator configuration, or two or more smaller accelerators.

VI. DISCUSSION

The accelerator designs outlined in Secs. II, III, IV, and V produce electrical powers an order of magnitude greater than are presently available. Such powers would enable high-energy-density physics experiments to be conducted over heretofore inaccessible parameter regimes.

Even higher powers could be achieved by conceptually straightforward upgrades to the designs described above. Such upgrades include the following.

(i) *Increasing the outer diameter of the accelerator tank.*—This would allow an increase in the number of electrical-pulse generators (such as the Marx-based pulsers or LTD modules described in this article), which would increase the peak forward-going power $P_{f,i}$ that is launched at the input to the radial-transmission-line impedance transformers.

(ii) *Replacing the electrical-pulse generators described herein with more powerful versions of these drivers.*—The Marx-based pulsers assumed in Secs. II and III could be upgraded by increasing the voltage at which the Marxes, intermediate stores, and laser-triggered gas switches oper-

ate. Alternatively, the simple transmission-line pulsers assumed for the water section of Fig. 1 could be replaced with Blumleins, which might allow an increase in the forward-going power. The LTD modules assumed in Secs. IV and V could be improved by increasing the power produced by each LTD cavity, or increasing the number of LTD cavities per module.

(iii) *Increasing the number of water-transmission-line levels above the 6 indicated in Figs.* 1, 3, *and* 4.—Increasing the number from 6 to 8 would increase the forward-going power $P_{f,i}$ by 33%, and according to Eq. (40), the peak pinch current I by as much as 11%.

(iv) *Increasing the accelerator efficiency.*—The efficiency could be increased by reducing the series resistance of the electrical-pulse generators, increasing the water resistivity (of the water section) above 3 MΩ-cm, developing a transformer-impedance profile that is more efficient than the exponential profiles assumed for this article, or reducing the value of the initial stack-MITL inductance L_s at which the accelerator could be operated reliably.

(v) *Optimizing the shape of the forward-going voltage pulse in the radial transformers.*—As discussed by Struve and McDaniel [71], the optimum shape is that which results in a square voltage pulse at the stack. For a given value of energy in the electrical-power pulse produced by the accelerator, flattening the voltage at the stack would minimize the peak stack voltage and hence the requisite value of L_s, which would in turn maximize the peak current that could be delivered to the load.

(vi) *Decreasing the temporal width of the power pulse produced by the electrical-pulse generators.*—The pulse could be decreased by adding pulse-compression circuitry to the architecture. Decreasing the pulse might increase the peak electrical power of the accelerator; it might also improve the radiation efficiency of the accelerator-pinch system, as discussed in Ref. [42].

It is clear, of course, that although the upgrades listed above are *conceptually* straightforward, each of these would require a significant effort to be implemented successfully.

APPENDIX A: POWER AND ENERGY EFFICIENCIES OF EXPONENTIAL IMPEDANCE TRANSFORMERS

The power and energy efficiencies of a transmission-line impedance transformer are functions of the frequency spectrum of the forward-going-voltage pulse being transformed, the one-way transit time of the transformer, the transformer's impedance profile, the impedance of the pulse generator at the transformer input, the impedance of the load at the transformer output, and dissipative losses in the dielectric and electrodes of the transformer. For these reasons the efficiencies of a transformer might best be determined *numerically*.

Nevertheless, we review in this Appendix an *analytic* result [106] that is obtained for the power efficiency of a transmission-line transformer with an *exponential* impedance profile; i.e., a profile that satisfies Eq. (1). The analytic result is useful for estimating the efficiency of such a transformer in the high-frequency limit. We also compare predictions of the analytic result with those obtained numerically.

We make the simplifying assumption that the forward-going *voltage* pulse in the transformer has a dominant angular frequency, which we label as ω_v. We label the impedance of the transformer at its input as $Z_{t,i}$, the impedance at the output as $Z_{t,o}$, and the one-way transit time of the transformer as τ. When

$$\omega_v^2 \gg \frac{[\ln(Z_{t,o}/Z_{t,i})]^2}{4\tau^2} \tag{A1}$$

the *power* efficiency of the transformer is approximately given as follows [106]:

$$\frac{P_{f,o}}{P_{f,i}} = \exp\left(\frac{-[\ln(Z_{t,o}/Z_{t,i})]^2}{4\omega_v\tau}\right). \tag{A2}$$

The quantities $P_{f,i}$ and $P_{f,o}$ are the forward-going powers at the input and output of the transformer, respectively. Equation (A2) can be inferred from the results presented in Sec. 3.4.5.1 of Ref. [106]. The above equation is valid when the generator impedance at the transformer input equals $Z_{t,i}$, the load impedance at the output equals $Z_{t,o}$, and dissipative losses in the dielectric and conductors can be neglected [106].

According to Eq. (A2) such a transformer is most efficient for frequencies that satisfy both Eq. (A1) and the

following relation:

$$\omega_v \gg \frac{[\ln(Z_{t,o}/Z_{t,i})]^2}{4\tau}. \qquad \text{(A3)}$$

Consequently, the transformer described above serves as a high-pass filter [105,106]. However, arbitrarily low frequencies are still transmitted because conductors connect the input and output, which is unlike other high-pass filters [106].

Since

$$\omega_v = \frac{a}{\tau_v}, \qquad \text{(A4)}$$

where a is a constant and τ_v is the full-width at half maximum of the forward-going voltage pulse, Eq. (A2) can be expressed as

$$\frac{P_{f,o}}{P_{f,i}} = \exp\left(\frac{-\tau_v[\ln(Z_{t,o}/Z_{t,i})]^2}{4a\tau}\right). \qquad \text{(A5)}$$

Hence the power efficiency is a function of the impedance ratio $Z_{t,o}/Z_{t,i}$ and the ratio of the voltage-pulse width to the transformer length τ_v/τ.

Table III compares predictions of Eq. (A2) to numerical results [127] for several exponential transformers. Table III assumes that the forward-going voltage at the input to the transformer is proportional to $\sin(\omega_v t)$ for $0 \leq \omega_v t \leq \pi$, and that the voltage equals 0 at all other times. (In this case, the constant $a = 2\pi/3$.) Table III assumes $\omega_v = 1.40 \times 10^7 \text{ s}^{-1}$, which is approximately the dominant angular frequency of the forward-going voltage pulse for both the Marx- and LTD-based accelerators described in Secs. III A

and VA, respectively. As suggested by Table III, Eq. (A2) is reasonably consistent with the numerical results.

APPENDIX B: OPTIMUM IMPEDANCE OF A TRANSMISSION LINE CONNECTED TO THE OUTPUT OF A SWITCH

In this Appendix we consider a transmission line that delivers an electrical-power pulse to a second transmission line through a closed gas switch. (The following discussion is, of course, valid for other types of switches.) We assume that the forward-going power pulse in the first line is incident upon the switch, and estimate the impedance of the second line that maximizes the forward-going power in the second.

We assume that the forward-going pulse in the first line has pulse width τ_g, and that the closed switch has inductance L_g and resistance R_g. We label the impedances of the first and second transmission lines as Z_1 and Z_2, respectively. We seek the value of Z_2 that maximizes the forward-going power in the second line.

Neglecting pulse-shape effects, we make the simplifying assumption that the total *effective* series resistance of the switch R_{eff} can be approximated as follows:

$$R_{\text{eff}} \sim \frac{L_g}{\tau_g} + R_g. \qquad \text{(B1)}$$

Consequently the first transmission line is in effect terminated in a load with impedance

$$Z_{\text{load}} = R_{\text{eff}} + Z_2. \qquad \text{(B2)}$$

Assuming that the forward-going pulse in the first line has peak voltage V_1, the peak voltage across the load is

TABLE III. Power and energy efficiencies of several transmission-line transformers with exponential impedance profiles. In each case it is assumed that the pulse generator that drives the transformer has impedance $Z_{t,\,i}$, and that the transformer is terminated in a load with impedance $Z_{t,\,o}$. Hence the efficiencies given below are valid only under these idealized conditions. All the calculations assume that the dominant angular frequency of the forward-going voltage pulse $\omega_v = 1.40 \times 10^7 \text{ s}^{-1}$. The efficiencies are given for different impedance ratios, transformer lengths, and water resistivities. The power efficiencies calculated analytically are given by Eq. (A2); the numerical efficiencies are obtained using the SCREAMER circuit code [127]. The transformers described in the 1st and 5th rows are those assumed for the Marx- and LTD-based accelerators described in Secs. III A and VA, respectively. [No analytic predictions are given for these two cases since Eq. (A2) assumes the water resistivity $\rho_w = \infty$.] For each of the six cases that assume $\rho_w = \infty$, the analytic power efficiency is in reasonable agreement with the numerical result.

Transformer design	Transformer power efficiency predicted by Eq. (A2)	Transformer power efficiency calculated numerically [127]	Transformer energy efficiency calculated numerically [127]
$Z_{t,i} = 0.0162\ \Omega$, $Z_{t,o} = 0.260\ \Omega$, $\tau = 1230$ ns, $\rho_w = 3$ MΩ-cm		83%	81%
$Z_{t,i} = 0.0162\ \Omega$, $Z_{t,o} = 0.260\ \Omega$, $\tau = 1230$ ns, $\rho_w = \infty$	89%	89%	87%
$Z_{t,i} = 0.0162\ \Omega$, $Z_{t,o} = 0.520\ \Omega$, $\tau = 1230$ ns, $\rho_w = \infty$	84%	84%	81%
$Z_{t,i} = 0.0162\ \Omega$, $Z_{t,o} = 0.260\ \Omega$, $\tau = 615$ ns, $\rho_w = \infty$	80%	81%	77%
$Z_{t,i} = 0.0339\ \Omega$, $Z_{t,o} = 0.360\ \Omega$, $\tau = 1010$ ns, $\rho_w = 3$ MΩ-cm		86%	84%
$Z_{t,i} = 0.0339\ \Omega$, $Z_{t,o} = 0.360\ \Omega$, $\tau = 1010$ ns, $\rho_w = \infty$	91%	91%	88%
$Z_{t,i} = 0.0339\ \Omega$, $Z_{t,o} = 0.720\ \Omega$, $\tau = 1010$ ns, $\rho_w = \infty$	85%	85%	82%
$Z_{t,i} = 0.0339\ \Omega$, $Z_{t,o} = 0.360\ \Omega$, $\tau = 505$ ns, $\rho_w = \infty$	82%	83%	79%

$$V_{\text{load}} = V_1 \left(\frac{2Z_{\text{load}}}{Z_{\text{load}} + Z_1} \right). \qquad (B3)$$

The peak voltage across Z_2 is

$$V_2 = V_{\text{load}} \left(\frac{Z_2}{Z_{\text{load}}} \right) = V_1 \left(\frac{2Z_2}{Z_{\text{load}} + Z_1} \right). \qquad (B4)$$

The peak forward-going power across Z_2 is

$$\frac{V_2^2}{Z_2} = V_1^2 \frac{4Z_2}{(Z_{\text{load}} + Z_1)^2}. \qquad (B5)$$

The ratio of the forward-going power in the second line to that in the first is

$$\frac{V_2^2/Z_2}{V_1^2/Z_1} = \frac{4Z_2 Z_1}{(Z_{\text{load}} + Z_1)^2} = \frac{4Z_2 Z_1}{(R_{\text{eff}} + Z_2 + Z_1)^2}. \qquad (B6)$$

We differentiate the rightmost expression with respect to Z_2 to find that the above ratio is maximized when

$$Z_2(\text{optimum}) = Z_1 + R_{\text{eff}} = Z_1 + \frac{L_g}{\tau_g} + R_g. \qquad (B7)$$

When Z_2 is given by the above expression, combining Eqs. (B2), (B4), and (B7) gives

$$V_2 = V_1 \left(\frac{2Z_2}{Z_{\text{load}} + Z_1} \right) = V_1. \qquad (B8)$$

Since Eqs. (B1)–(B8) neglect pulse-shape effects, the equations are, in general, accurate to at most first order.

APPENDIX C: EFFECTIVE VALUES OF THE PEAK PINCH CURRENT AND PINCH IMPLOSION TIME

The circuit calculations presented in this article assume that the implosion of a z pinch can be approximated as that of a very-thin perfectly stable annular shell, and that the implosion has perfect cylindrical symmetry. The calculations also assume that the pinch-radius convergence ratio is 10:1.

Under these conditions the imploded sheath (just before stagnation) of the pinch can be uniquely described by only four independent variables. We are free to choose two of these to be the pinch length ℓ and the initial pinch radius R. The remaining two can be the final implosion velocity v_p and the final pinch kinetic energy E_k:

$$v_p \quad \text{and} \quad E_k. \qquad (C1)$$

We can instead choose the remaining two variables to be the total pinch mass m and E_k:

$$m \quad \text{and} \quad E_k. \qquad (C2)$$

Another option is to use

$$v_p \quad \text{and} \quad m. \qquad (C3)$$

Only two of the variables v_p, E_k, and m are independent since

$$\tfrac{1}{2} m v_p^2 = E_k. \qquad (C4)$$

Instead of the two independent variables given by either Eqs. (C1), (C2), or (C3), it is customary to use the peak pinch current I and the implosion time τ_i:

$$I \quad \text{and} \quad \tau_i. \qquad (C5)$$

Members of the z-pinch community often use the variables I and τ_i when comparing the results of various circuit simulations (that use the ideal pinch model described above) to each other. However, it is clear that I and τ_i are meaningful for such comparisons only when the *shape* of the load currents under consideration are *mathematically similar*. When the shapes are significantly dissimilar, it is necessary to revert to the more fundamental quantities v_p, E_k, and m. The variables I and τ_i serve only as proxies for the more fundamental variables, and can do so in a meaningful manner only to the extent that the simulations under consideration produce *similar* load-current pulse shapes.

When comparing simulations that do not produce mathematically similar current pulses, we can define an *effective* peak pinch current and an *effective* pinch implosion time. For the discussions in this article we define these quantities as follows:

$$I_{\text{eff}} = 2357 \left(\frac{E_k}{\ell} \right)^{1/2}, \qquad (C6)$$

$$\tau_{i,\text{eff}} = 4.465 \frac{R}{v_p}, \qquad (C7)$$

The constants on the right-hand sides of the above two equations were arbitrarily chosen to give results consistent with those obtained on the Z accelerator [40,42], which are presented in the first columns of Tables I and II. Equations (C6) and (C7) are consistent with Eq. (2).

Equation (C6) guarantees that two simulations with the same effective peak current have the same final pinch kinetic energy per unit length. Equation (C7) guarantees that two simulations with the same initial radius and same effective implosion time have the same final pinch velocity. Of course, it is to be remembered that, for a given pinch convergence ratio, the *fundamental* variables that uniquely describe the final imploded pinch are ℓ, R, v_p, E_k, and m, and that only two of the last three variables are independent.

APPENDIX D: OPTIMUM OUTPUT IMPEDANCE OF THE INTERNAL TRANSMISSION LINE OF AN LTD MODULE

We present here the optimum *output* impedance of the concentric transmission line that is located within, and is driven by, an LTD module.

For this calculation we assume the LTD circuit model illustrated by Fig. 5. This model, which is accurate to first

W. A. STYGAR *et al.*

Phys. Rev. ST Accel. Beams **10,** 030401 (2007)

order, is proposed by Mazarakis and colleagues in Refs. [76,79,86]. (Considerably more complete LTD circuit models are proposed by Kim and colleagues in Ref. [94] and Leckbee and co-workers in Ref. [99].)

Figure 5 represents an LTD module that consists of three LTD cavities connected in series. For an LTD module with n_{cav} cavities, we have that

$$R_{\mathrm{mod}} = n_{\mathrm{cav}} R_{\mathrm{cav}}, \tag{D1}$$

$$L_{\mathrm{mod}} = n_{\mathrm{cav}} L_{\mathrm{cav}}, \tag{D2}$$

$$C_{\mathrm{mod}} = C_{\mathrm{cav}}/n_{\mathrm{cav}}, \tag{D3}$$

$$Z_{\mathrm{mod}} = n_{\mathrm{cav}} Z_{\mathrm{cav}}. \tag{D4}$$

The quantities R_{cav}, L_{cav}, and C_{cav} are the series resistance, inductance, and capacitance, respectively, of a single LTD cavity. The quantities R_{mod}, L_{mod}, and C_{mod} are the series resistance, inductance, and capacitance, respectively, of an LTD module with n_{cav} cavities. The quantity Z_{cav} is the impedance of the transmission-line segment driven by the *first* cavity; Z_{mod} is the impedance of the segment driven by the *final* cavity.

As discussed in Sec. IV B, each of the cavities considered herein contains 80 capacitors and 40 switches. (These are represented in Fig. 5 by a single capacitor and a single switch.) The circuit model of Fig. 5 and Eqs. (D1)–(D4) assumes that the switches of a given cavity close at a time that is τ_{cav} later than the closure of the switches in the cavity immediately to the left, where τ_{cav} is the time it takes an electromagnetic pulse to propagate the length of a single cavity. Hence, τ_{cav} is the one-way transit time of a single transmission-line segment. (We assume here that all the cavities, and all the transmission-line segments, have the same electrical length.)

For an n_{cav}-cavity version of Fig. 5(c), it is well known that the charge on the capacitance C_{mod} (which we label as Q_{mod}), and the current flowing through the circuit (which we label as I_{mod}) are, after all the switches have closed, given as follows:

$$Q_{\mathrm{mod}}(t) = A e^{-\alpha t} \cos(\omega t + \beta), \tag{D5}$$

$$I_{\mathrm{mod}}(t) = -\omega A e^{-\alpha t} \sin(\omega t + \beta) - \alpha A e^{-\alpha t} \cos(\omega t + \beta), \tag{D6}$$

where

$$A \equiv \frac{Q_{\mathrm{mod}}(t=0)}{\cos\beta} = \frac{C_{\mathrm{mod}} V_{\mathrm{mod}}}{\cos\beta}, \tag{D7}$$

$$V_{\mathrm{mod}} \equiv \frac{Q_{\mathrm{mod}}(t=0)}{C_{\mathrm{mod}}} = n_{\mathrm{cav}} V_{\mathrm{cav}}, \tag{D8}$$

$$\alpha \equiv \frac{R_{\mathrm{mod}} + Z_{\mathrm{mod}}}{2L_{\mathrm{mod}}}, \tag{D9}$$

$$\omega^2 \equiv \frac{1}{L_{\mathrm{mod}} C_{\mathrm{mod}}} - \frac{(R_{\mathrm{mod}} + Z_{\mathrm{mod}})^2}{4L_{\mathrm{mod}}^2}, \tag{D10}$$

$$\beta \equiv \arctan\left(\frac{-\alpha}{\omega}\right). \tag{D11}$$

Equations (D5)–(D11) are valid whenever $\omega > 0$. The quantity V_{cav} is the *initial* charge voltage across capacitance C_{cav}. Equation (D8) assumes that the initial voltage is the same for each of the n_{cav} cavities.

The power delivered to the transmission-line output impedance Z_{mod} is given by

$$P_{\mathrm{mod}} = I_{\mathrm{mod}}^2 Z_{\mathrm{mod}}. \tag{D12}$$

In this article we define the *optimum* value of Z_{mod} to be that which maximizes the peak value (in time) of P_{mod}.

To determine $Z_{\mathrm{mod,opt}}$ we use Eqs. (D1)–(D12) and dimensional analysis to observe that it may be possible to express the ratio $Z_{\mathrm{mod,opt}}/(L_{\mathrm{mod}}/C_{\mathrm{mod}})^{1/2}$ as an explicit function of only the ratio $R_{\mathrm{mod}}/(L_{\mathrm{mod}}/C_{\mathrm{mod}})^{1/2}$:

$$\frac{Z_{\mathrm{mod,\ opt}}}{(L_{\mathrm{mod}}/C_{\mathrm{mod}})^{1/2}} = f\left(\frac{R_{\mathrm{mod}}}{(L_{\mathrm{mod}}/C_{\mathrm{mod}})^{1/2}}\right). \tag{D13}$$

Using Eqs. (D1)–(D13) we calculated $Z_{\mathrm{mod,opt}}/(L_{\mathrm{mod}}/C_{\mathrm{mod}})^{1/2}$ numerically at several values of $R_{\mathrm{mod}}/(L_{\mathrm{mod}}/C_{\mathrm{mod}})^{1/2}$. The results are summarized in Fig. 7. A least-squares fit to a line finds that

$$Z_{\mathrm{mod,opt}} = 1.10\sqrt{\frac{L_{\mathrm{mod}}}{C_{\mathrm{mod}}}} + 0.80 R_{\mathrm{mod}}. \tag{D14}$$
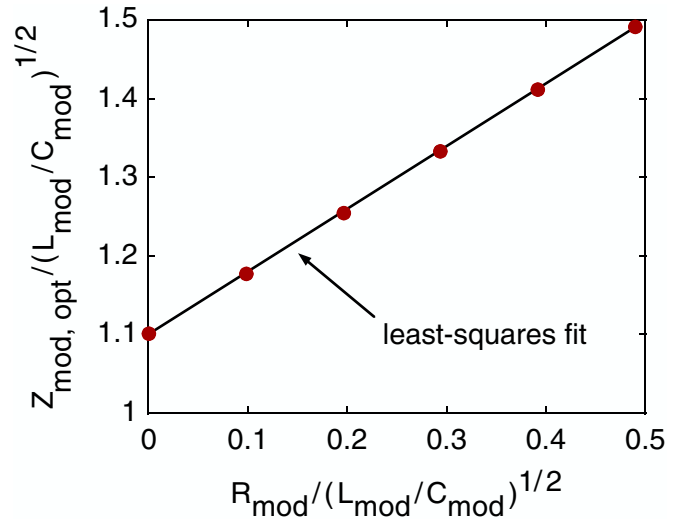

FIG. 7. (Color) The ratio $Z_{\mathrm{mod,opt}}/(L_{\mathrm{mod}}/C_{\mathrm{mod}})^{1/2}$ calculated numerically at six different values of $R_{\mathrm{mod}}/(L_{\mathrm{mod}}/C_{\mathrm{mod}})^{1/2}$. The numerical results suggest a linear relationship. The solid black line is a least-squares fit to a line; the slope and intercept are 0.80 and 1.10, respectively.

Combining Eqs. (D1)–(D3) and (D14) gives

$$Z_{\mathrm{mod,opt}} = n_{\mathrm{cav}}\left(1.10\sqrt{\frac{L_{\mathrm{cav}}}{C_{\mathrm{cav}}}} + 0.80R_{\mathrm{cav}}\right). \qquad (\mathrm{D15})$$

Equation (D15) and Fig. 5 suggest that when $Z_{\mathrm{mod}} = Z_{\mathrm{mod,opt}}$, the impedance of the kth transmission-line segment is given by

$$Z_{k,\ \mathrm{opt}} = k\left(1.10\sqrt{\frac{L_{\mathrm{cav}}}{C_{\mathrm{cav}}}} + 0.80R_{\mathrm{cav}}\right). \qquad (\mathrm{D16})$$

Equations (D15) and (D16) are correct to $<1\%$ whenever $\omega > 0$, and the LTD module can be modeled as suggested by Eqs. (D1)–(D11) and Fig. 5.

---

[1] W. L. Baker, M. C. Clark, J. H. Degnan, G. F. Kiuttu, C. R. McClenahan, and R. E. Reinovsky, J. Appl. Phys. **49**, 4694 (1978).

[2] W. W. Hsing, R. Coats, D. H. McDaniel, and R. B. Spielman, in *Proceedings of the 5th IEEE International Pulsed Power Conference*, edited by M. F. Rose and P. J. Turchi (IEEE, Piscataway, NJ, 1985), p. 704.

[3] T. P. Wright, D. H. McDaniel, R. W. Stinnett, W. W. Hsing, R. B. Spielman, M. A. Hedemann, P. W. Spence, K. E. Nielsen, J. Kishi, and R. G. Sears, in *Proceedings of the 5th IEEE International Pulsed Power Conference*, Ref. [2], p. 493.

[4] R. B. Spielman, D. L. Hanson, M. A. Palmer, M. K. Matzen, T. W. Hussey, and J. M. Peek, J. Appl. Phys. **57**, 830 (1985).

[5] R. B. Spielman, W. W. Hsing, and D. L. Hanson, Rev. Sci. Instrum. **59**, 1804 (1988).

[6] W. B. Moore, R. W. Stinnett, and D. H. McDaniel, in *Proceedings of the 5th IEEE International Pulsed Power Conference*, Ref. [2], p. 315.

[7] P. Sincerny *et al.*, in *Proceedings of the 5th IEEE International Pulsed Power Conference*, Ref. [2], p. 151.

[8] D. D. Bloomquist, R. M. Stinnett, D. H. McDaniel, J. R. Lee, A. W. Sharpe, J. A. Halbleib, L. G. Shlitt, P. W. Spence, and P. Corcoran, in *Proceedings of the 6th IEEE International Pulsed Power Conference*, edited by P. J. Turchi and B. H. Bernstein (IEEE, Piscataway, NJ, 1987), p. 310.

[9] R. B. Spielman, R. J. Dukart, D. L. Hanson, B. A. Hammel, W. W. Hsing, M. K. Matzen, and J. L. Porter, in *Dense Z Pinches: Proceedings of the 2nd International Conference on Dense Z Pinches*, edited by N. R. Pereira, J. Davis, and N. Rostoker, AIP Conf. Proc. No. 195 (AIP, Melville, New York, 1989), p. 3.

[10] V. P. Smirnov, E. V. Grabovskii, V. I. Zaytsev, S. V. Sakharov, S. L. Nedoseev, V. Ya. Tsarfin, and I. R. Yampolskii, in *Proceedings of the 8th International Conference on High-Power Particle Beams (Beams '90)*, edited by B. N. Breizman and B. A. Knyazev (World Scientific, Singapore, 1990), p. 61.

[11] E. V. Grabovsky *et al.*, Proc. SPIE-Int. Soc. Opt. Eng. **4424**, 10 (2001).

[12] J. C. Cochrane *et al.*, in *Dense Z Pinches: Proceedings of the 3rd International Conference on Dense Z Pinches*, edited by M. Haines and A. Knight, AIP Conf. Proc. No. 299 (AIP, Melville, New York, 1994), p. 381.

[13] R. Hall, L. Rohlev, L. Earley, and J. Cochrane, Proc. SPIE-Int. Soc. Opt. Eng. **2611**, 227 (1996).

[14] D. L. Peterson, R. L. Bowers, K. D. McLenithan, C. Deeney, G. A. Chandler, R. B. Spielman, M. K. Matzen, and N. F. Roderick, Phys. Plasmas **5**, 3302 (1998).

[15] I. H. Mitchell, J. M. Bayley, J. P. Chittenden, J. F. Worley, A. E. Dangor, and M. G. Haines, Rev. Sci. Instrum. **67**, 1533 (1996).

[16] B. S. Bauer, V. L. Kantsyrev, F. Winterberg, A. S. Shlyaptseva, R. C. Mancini, H. Li, and A. Oxner, in *Dense Z Pinches: Proceedings of the 4th International Conference on Dense Z Pinches*, edited by N. Pereira, J. Davis, and P. Pulsifer, AIP Conf. Proc. No. 409 (AIP, Melville, New York, 1997), p. 153.

[17] B. S. Bauer *et al.*, in *Proceedings of the 12th IEEE International Pulsed Power Conference*, edited by C. Stallings and H. Kirbie (IEEE, Piscataway, NJ, 1999), p. 1045.

[18] W. M. Parsons *et al.*, IEEE Trans. Plasma Sci. **25**, 205 (1997).

[19] R. B. Miller *et al.*, in *Proceedings of the 12th IEEE International Pulsed Power Conference*, Ref. [17], p. 484.

[20] P. Sincerny, K. Childers, D. Kortbawi, I. Roth, C. Stallings, J. Riordan, B. Hoffman, L. Schlitt, and C. Myers, in *Proceedings of the 11th IEEE International Pulsed Power Conference*, edited by G. Cooperstein and I. Vitkovitsky (IEEE, Piscataway, NJ, 1997), p. 698.

[21] W. Rix *et al.*, in *Proceedings of the 13th IEEE International Pulsed Power Conference*, edited by R. Reinovsky and M. Newton (IEEE, Piscataway, NJ, 2001), p. 573.

[22] R. B. Spielman *et al.*, in *Proceedings of the 11th IEEE International Pulsed Power Conference*, Ref. [20], p. 709.

[23] P. A. Corcoran, J. W. Douglas, I. D. Smith, P. W. Spence, W. A. Stygar, K. W. Struve, T. H. Martin, R. B. Spielman, and H. C. Ives, in *Proceedings of the 11th IEEE International Pulsed Power Conference*, Ref. [20], p. 466.

[24] R. J. Garcia, H. C. Ives, K. W. Struve, R. B. Spielman, T. H. Martin, M. L. Horry, R. Wavrik, and T. F. Jaramillo, in *Proceedings of the 11th IEEE International Pulsed Power Conference*, Ref. [20], p. 1614.

[25] H. C. Ives, D. M. Van De Valde, F. W. Long, J. W. Smith, R. B. Spielman, W. A. Stygar, R. W. Wavrick, and R. W. Shoup, in *Proceedings of the 11th IEEE International Pulsed Power Conference*, Ref. [20], p. 1602.

[26] M. A. Mostrom, T. P. Hughes, R. E. Clark, W. A. Stygar, and R. B. Spielman, in *Proceedings of the 11th IEEE International Pulsed Power Conference*, Ref. [20], p. 460.

[27] R. W. Shoup, F. Long, T. H. Martin, R. B. Spielman, W. A. Stygar, M. A. Mostrom, K. W. Struve, H. Ives, P. Corcoran, and I. Smith, in *Proceedings of the 11th IEEE International Pulsed Power Conference*, Ref. [20], p. 1608.

[28] I. D. Smith, P. A. Corcoran, W. A. Stygar, T. H. Martin, R. B. Spielman, and R. W. Shoup, in *Proceedings of the 11th IEEE International Pulsed Power Conference*, Ref. [20], p. 168.

[29] K. W. Struve, T. H. Martin, R. B. Spielman, W. A. Stygar, P. A. Corcoran, and J. W. Douglas, in *Proceedings of the 11th IEEE International Pulsed Power Conference*, Ref. [20], p. 162.

[30] W. A. Stygar *et al.*, in *Proceedings of the 11th IEEE International Pulsed Power Conference*, Ref. [20], p. 591.

[31] R. B. Spielman *et al.*, Phys. Plasmas **5**, 2105 (1998).

[32] J. D. Douglass, J. B. Greenly, D. A. Hammer, B. R. Kusse, L. M. Maxson, R. D. McBride, and S. Glidden, in *Proceedings of the 15th IEEE International Pulsed Power Conference* (IEEE, Piscataway, NJ, 2005).

[33] T. W. L. Sanford *et al.*, Phys. Rev. Lett. **77**, 5063 (1996).

[34] C. Deeney *et al.*, Phys. Rev. E **56**, 5945 (1997).

[35] J. L. Porter, Bull. Am. Phys. Soc. **42**, 1948 (1997).

[36] K. L. Baker *et al.*, Appl. Phys. Lett. **75**, 775 (1999).

[37] K. L. Baker, J. L. Porter, L. E. Ruggles, R. E. Chrien, and G. C. Idzorek, Rev. Sci. Instrum. **70**, 1624 (1999).

[38] K. L. Baker *et al.*, Rev. Sci. Instrum. **70**, 2012 (1999).

[39] K. L. Baker *et al.*, Phys. Plasmas **7**, 681 (2000).

[40] W. A. Stygar *et al.*, Phys. Rev. E **69**, 046403 (2004).

[41] M. E. Cuneo *et al.*, Phys. Rev. E **71**, 046406 (2005).

[42] W. A. Stygar *et al.*, Phys. Rev. E **72**, 026404 (2005).

[43] M. E. Cuneo *et al.*, Phys. Plasmas **13**, 056318 (2006).

[44] J. H. Hammer, M. Tabak, S. C. Wilks, J. D. Lindl, D. S. Bailey, P. W. Rambo, A. Toor, G. B. Zimmerman, and J. L. Porter, Jr., Phys. Plasmas **6**, 2129 (1999).

[45] R. J. Leeper *et al.*, Nucl. Fusion **39**, 1283 (1999).

[46] M. E. Cuneo, R. A. Vesey, J. H. Hammer, J. L. Porter, Jr., L. E. Ruggles, and W. W. Simpson, Laser Part. Beams **19**, 481 (2001).

[47] M. E. Cuneo *et al.*, Phys. Plasmas **8**, 2257 (2001).

[48] M. E. Cuneo *et al.*, Phys. Rev. Lett. **88**, 215004 (2002).

[49] G. R. Bennett *et al.*, Phys. Rev. Lett. **89**, 245002 (2002).

[50] D. L. Hanson *et al.*, Phys. Plasmas **9**, 2173 (2002).

[51] R. A. Vesey, M. E. Cuneo, G. R. Bennett, J. L. Porter, Jr., R. G. Adams, R. A. Aragon, P. K. Rambo, L. E. Ruggles, W. W. Simpson, and I. C. Smith, Phys. Rev. Lett. **90**, 035005 (2003).

[52] G. R. Bennett *et al.*, Phys. Plasmas **10**, 3717 (2003).

[53] R. A. Vesey, M. E. Cuneo, J. L. Porter, Jr., R. G. Adams, R. A. Aragon, P. K. Rambo, L. E. Ruggles, W. W. Simpson, I. C. Smith, and G. R. Bennett, Phys. Plasmas **10**, 1854 (2003).

[54] R. A. Vesey, M. E. Cuneo, G. R. Bennett, D. Hanson, J. L. Porter, L. E. Ruggles, W. W. Simpson, T. A. Mehlhorn, and S. E. Wunsch, Bull. Am. Phys. Soc. **48**, 207 (2003).

[55] R. E. Olson *et al.*, Fusion Technol. **35**, 260 (1999).

[56] T. W. L. Sanford *et al.*, Phys. Rev. Lett. **83**, 5511 (1999).

[57] J. E. Bailey *et al.*, Phys. Rev. Lett. **92**, 085002 (2004).

[58] C. L. Ruiz *et al.*, Phys. Rev. Lett. **93**, 015001 (2004).

[59] R. E. Olson, Fusion Sci. Technol. **47**, 1147 (2005).

[60] C. L. Olson, in *Landholt-Boernstein Handbook on Energy Technologies*, edited by W. Martienssen, Vol. VIII/3 of Fusion Technologies, edited by K. Heinloth (Springer-Verlag, Berlin-Heidelberg, 2005).

[61] R. A. Vesey *et al.* (to be published).

[62] M. D. Rosen, Phys. Plasmas **3**, 1803 (1996).

[63] M. K. Matzen, Phys. Plasmas **4**, 1519 (1997).

[64] M. A. Liberman, J. S. DeGroot, A. Toor, and R. B. Spielman, *Physics of High-Density Z-Pinch Plasmas* (Springer, New York, 1999).

[65] D. D. Ryutov, M. S. Derzon, and M. K. Matzen, Rev. Mod. Phys. **72**, 167 (2000).

[66] J. E. Bailey *et al.*, Phys. Plasmas **9**, 2186 (2002).

[67] J. M. Foster, B. H. Wilde, P. A. Rosen, T. S. Perry, M. Fell, M. J. Edwards, B. F. Lasinski, R. E. Turner, and M. L. Gittings, Phys. Plasmas **9**, 2251 (2002).

[68] T. W. L. Sanford *et al.*, Plasma Phys. Controlled Fusion **46**, B423 (2004).

[69] J. J. Ramirez, in *Proceedings of the 10th IEEE International Pulsed Power Conference*, edited by W. Baker and G. Cooperstein (IEEE, Piscataway, NJ, 1995), p. 91.

[70] T. H. Martin (unpublished).

[71] K. W. Struve and D. H. McDaniel, in *Proceedings of the 12th International Conference on High-Power Particle Beams (Beams '98)*, edited by M. Markovits and J. Shiloh (IEEE, Haifa, Isreal, 1998), p. 334.

[72] P. Sincerny, M. Danforth, C. Gilbert, A. R. Miller, T. Naff, W. Rix, C. Stallings, E. Waisman, and L. Schlitt, in *Proceedings of the 12th IEEE International Pulsed Power Conference*, Ref. [17], p. 479.

[73] K. W. Struve, J. P. Corley, D. L. Johnson, D. H. McDaniel, R. B. Spielman, and W. A. Stygar, in *Proceedings of the 12th IEEE International Pulsed Power Conference*, Ref. [17], p. 493.

[74] A. A. Kim and B. M. Kovaltchuk, in *Proceedings of the 12th Symposium on High Current Electronics*, edited by G. Mesyats, B. Kovalchuk, and G. Remnev (Institute of High Current Electronics, Tomsk, Russia, 2000), p. 263.

[75] P. Corcoran, I. Smith, P. Spence, A. R. Miller, E. Waisman, C. Gilbert, W. Rix, P. Sincerny, L. Schlitt, and D. Bell, in *Proceedings of the 13th IEEE International Pulsed Power Conference*, Ref. [21], p. 577; I. Smith, P. Corcoran, A. R. Miller, V. Carboni, P. Sincerny, P. Spence, C. Gilbert, W. Rix, E. Waisman, L. Schlitt, and D. Bell, IEEE Trans. Plasma Sci. **30**, 1746 (2002).

[76] M. G. Mazarakis, R. B. Spielman, K. W. Struve, and F. W. Long, in *Proceedings of the 13th IEEE International Pulsed Power Conference*, Ref. [21], p. 587.

[77] D. H. McDaniel *et al.*, in *Dense Z Pinches: the Proceedings of the 5th International Conference on Dense Z Pinches*, edited by J. Davis, C. Deeney, and N. Pereira, AIP Conf. Proc. No. 651 (AIP, Melville, NY, 2002), p. 23.

[78] P. Spence *et al.*, in *Dense Z Pinches: the Proceedings of the 5th International Conference on Dense Z Pinches*, Ref. [77], p. 43.

[79] M. G. Mazarakis, W. E. Fowler, F. W. Long, D. H. McDaniel, C. L. Olson, S. T. Rogowski, R. A. Sharpe, and K. W. Struve, in *Proceedings of the 15th IEEE International Pulsed Power Conference*, Ref. [32].

[80] B. M. Kovalchuk, V. A. Vizir, A. A. Kim, E. V. Kumpjak, S. V. Loginov, A. N. Bastrikov, V. V. Chervjakov, N. V. Tsou, Ph. Monjaux, and D. Huet, Sov. Izw. Vuzov. Phys. **40**, 25 (1997).

[81] A. N. Bastrikov *et al.*, in *Proceedings of the 11th IEEE International Pulsed Power Conference*, Ref. [20], p. 489.

[82] A. A. Kim *et al.*, in *Proceedings of the 11th IEEE International Pulsed Power Conference*, Ref. [20], p. 862.

[83] B. M. Kovalchuk, in *Proceedings of the 11th IEEE International Pulsed Power Conference*, Ref. [20], p. 59.

[84] D. H. McDaniel and R. B. Spielman (unpublished).

[85] A. A. Kim, B. M. Kovalchuk, E. V. Kumpjak, and N. V. Zoi, in *Proceedings of the 12th IEEE International Pulsed Power Conference*, Ref. [17], p. 955.

[86] M. G. Mazarakis and R. B. Spielman, in *Proceedings of the 12th IEEE International Pulsed Power Conference*, Ref. [17], p. 412.

[87] A. A. Kim, B. M. Kovalchuk, A. N. Bastrikov, V. G. Durakov, S. N. Volkov, and V. A. Sinebryukhov, in *Proceedings of the 13th IEEE International Pulsed Power Conference*, Ref. [21], p. 1491.

[88] B. M. Kovalchuk, A. A. Kim, E. V. Kumpjak, N. V. Zoi, and V. B. Zorin, in *Proceedings of the 13th IEEE International Pulsed Power Conference*, Ref. [21], p. 1488.

[89] A. A. Kim, A. N. Bastrikov, S. N. Volkov, V. G. Durakov, B. M. Kovalchuk, and V. A. Sinebryukhov, in *Proceedings of the 14th International Conference on High-Power Particle Beams (Beams 2002)*, edited by T. A. Mehlhorn and M. A. Sweeney, AIP Conf. Proc. No. 650 (AIP, Melville, NY, 2002), p. 81.

[90] A. N. Bastrikov *et al.*, Laser Part. Beams **21**, 295 (2003).

[91] A. A. Kim, A. N. Bastrikov, S. N. Volkov, V. G. Durakov, B. M. Kovalchuk, and V. A. Sinebryukhov, in *Proceedings of the 14th IEEE International Pulsed Power Conference*, edited by M. Giesselmann and A. Neuber (IEEE, Piscataway, NJ, 2003), p. 853.

[92] B. M. Kovalchuk, A. A. Kim, E. V. Kumpjak, and N. V. Tsou, in *Proceedings of the 14th IEEE International Pulsed Power Conference*, Ref. [91], p. 1455.

[93] D. V. Rose, D. R. Welch, B. V. Oliver, J. E. Maenchen, D. C. Rovang, D. L. Johnson, A. A. Kim, and B. M. Kovalchuk, in *Proceedings of the 14th IEEE International Pulsed Power Conference*, Ref. [91], p. 845.

[94] A. A. Kim, A. N. Bastrikov, S. N. Volkov, V. G. Durakov, B. N. Kovalchuk, and V. A. Synebrukhov, in *Proceedings of the 13th International Symposium on High Current Electronics*, edited by B. Kovalchuk and G. Remnev (Institute of High Current Electronics, Tomsk, Russia, 2004), p. 141.

[95] V. A. Vizir, A. D. Maksimenko, V. I. Manylov, and G. V. Smorudov, in *Proceedings of the 13th International Symposium on High Current Electronics*, Ref. [94], p. 198.

[96] J. Leckbee, J. Maenchen, S. Portillo, S. Corodova, I. Molina, D. L. Johnson, D. V. Rose, A. A. Kim, R. Chavez, and D. Ziska, in *Proceedings of the 15th IEEE International Pulsed Power Conference*, Ref. [32].

[97] J. Leckbee, J. Maenchen, S. Portillo, S. Cordova, I. Molina, D. L. Johnson, A. A. Kim, R. Chavez, and D. Ziska, in *Proceedings of the 15th IEEE International Pulsed Power Conference*, Ref. [32].

[98] S. T. Rogowski, W. E. Fowler, M. G. Mazarakis, C. L. Olson, D. H. McDaniel, K. W. Struve, and R. A. Sharpe, in *Proceedings of the 15th IEEE International Pulsed Power Conference*, Ref. [32].

[99] J. J. Leckbee, J. E. Maenchen, D. L. Johnson, S. Portillo, D. M. Van De Valde, D. V. Rose, and B. V. Oliver, IEEE Trans. Plasma Sci. **34**, 1888 (2006).

[100] D. V. Rose, D. R. Welch, B. V. Oliver, J. J. Leckbee, J. E. Maenchen, D. L. Johnson, A. A. Kim, B. M. Kovalchuk, and V. A. Sinebryukhov, IEEE Trans. Plasma Sci. **34**, 1879 (2006).

[101] A. A. Kim *et al.*, in *Proceedings of the 14th International Symposium on High Current Electronics*, edited by B. Kovalchuk and G. Remnev (Institute of High Current Electronics, Tomsk, Russia, 2006), p. 297.

[102] M. G. Mazaraskis, W. E. Fowler, D. H. McDaniel, A. A. Kim, C. L. Olson, S. T. Rogowski, R. A. Sharpe, and K. W. Struve, in *Proceedings of the 14th International Symposium on High Current Electronics*, Ref. [101], p. 226.

[103] I. D. Smith, Phys. Rev. ST Accel. Beams **7**, 064801 (2004).

[104] T. H. Martin, J. P. VanDevender, D. L. Johnson, D. H. McDaniel, and M. Aker, in *Proceedings of the International Topical Conference on Electron Beam Research and Technology*, edited by Sandia National Labs (Sandia Labs, Albuquerque, NM, 1975), p. 450.

[105] R. A. Petr, W. C. Nunnally, C. V. Smith, Jr., and M. H. Clark, Rev. Sci. Instrum. **59**, 132 (1988).

[106] I. A. D. Lewis and F. H. Wells, *Millimicrosecond Pulse Techniques* (Pergamon Press, New York, 1959).

[107] K. Pendergraft and R. Pieper, J. Acoust. Sci. Am. **94**, 580 (1993).

[108] D. H. McDaniel, R. W. Stinnett, and I. D. Smith, Bull. Am. Phys. Soc. **25**, 1017 (1980).

[109] P. Sincerny *et al.*, in *Proceedings of the 5th IEEE International Pulsed Power Conference*, Ref. [2], p. 151.

[110] R. B. Spielman, P. Corcoran, J. Fockler, H. Kishi, and P. W. Spence, in *Proceedings of the 7th IEEE International Pulsed Power Conference*, edited by B. H. Bernstein and J. P. Shannon (IEEE, Piscataway, NJ, 1989), p. 445.

[111] T. P. Hughes and R. E. Clark, Mission Research Corporation Report MRC/ABQ-R-1875, 1998 (NTIS Order Number PB2001-104866).

[112] T. P. Hughes and R. E. Clark, Mission Research Corporation Report MRC/ABQ-R-2005, 2000 (NTIS Order Number PB2001-104868).

[113] T. P. Hughes, R. E. Clark, B. V. Oliver, R. A. St. John, and W. A. Stygar, Mission Research Corporation Report MRC/ABQ-R-2066, 2002 (NTIS Order Number PB2003-100707).

[114] T. D. Pointon, W. A. Stygar, R. B. Spielman, H. C. Ives, and K. W. Struve, Phys. Plasmas **8**, 4534 (2001).

[115] T. P. Hughes, R. E. Clark, B. V. Oliver, T. D. Pointon, and W. A. Stygar, in *Proceedings of the 14th IEEE International Pulsed Power Conference*, Ref. [91], p. 622.

[116] D. V. Rose, D. Welch, T. Hughes, R. Clark, and W. A. Stygar, in Proceedings of the 16th IEEE International Pulsed Power Conference (IEEE, Piscataway, NJ, to be published).

[117] D. V. Rose, D. Welch, T. Hughes, R. Clark, and W. A. Stygar (unpublished).

[118] J. C. Martin, in *J. C. Martin on Pulsed Power*, edited by T. H. Martin, A. H. Guenther, and M. Kristiansen (Plenum, New York, 1996).

[119] G. E. Vogtlin and J. E. Vernazza, in *Proceedings of the 7th IEEE Pulsed Power Conference*, edited by R. White and B. H. Bernstein (IEEE, Piscataway, NJ, 1989), p. 808.

[120] W. A. Stygar *et al.*, Phys. Rev. ST Accel. Beams **8**, 050401 (2005).

[121] W. A. Stygar *et al.*, Phys. Rev. ST Accel. Beams **7**, 070401 (2004).

[122] W. A. Stygar *et al.*, Phys. Rev. ST Accel. Beams **9**, 070401 (2006).

[123] E. L. Neau, J. F. Seamen, D. D. Bloomquist, S. R. Babcock, L. X. Schneider, and B. R. Sujka, in *Proceedings of the 5th IEEE International Pulsed Power Conference*, Ref. [2], p. 772.

[124] K. W. Struve, J. Corley, and D. L. Johnson (unpublished).

[125] L. X. Schneider and G. J. Lockwood, in *Proceedings of the 5th IEEE International Pulsed Power Conference*, Ref. [2], p. 780.

[126] M. E. Cuneo (unpublished).

[127] M. L. Kiefer and M. M. Widner, in *Proceedings of the 5th IEEE International Pulsed Power Conference*, Ref. [2], p. 685.

[128] M. E. Cuneo (unpublished).

[129] A. A. Kim *et al.* (unpublished).

[130] M. G. Mazarakis, W. E. Fowler, and R. A. Sharpe (unpublished).

[131] A. A. Kim (private communication).